frontiers in
MICROBIOLOGY

MINI REVIEW ARTICLE
published: 30 January 2012
doi: 10.3389/fmicb.2012.00014

Cell tropism and pathogenesis of measles virus in monkeys

Sei-ich Kato, Kyosuke Nagata and Kaoru Takeuchi*

Division of Biomedical Science, Department of Infection Biology, Faculty of Medicine, University of Tsukuba, Tsukuba, Japan

Edited by:
Yasuko Yokota, National Institute of Infectious Diseases, Japan

Reviewed by:
Yasuko Yokota, National Institute of Infectious Diseases, Japan
Michael D. Muehlebach, Paul-Ehrlich-Institut, Germany
Katsuhiro Komase, National Institute of Infectious Diseases, Japan

***Correspondence:**
Kaoru Takeuchi, Division of Biomedical Science, Department of Infection Biology, Faculty of Medicine, University of Tsukuba, 1-1-1 Tennodai, Tsukuba, Ibaraki 305-8575, Japan.
e-mail: ktakeuch@md.tsukuba.ac.jp

Measles virus (MV) is an enveloped negative strand RNA virus belonging to the family of Paramyxoviridae, genus *Morbillivirus*, and causes one of the most contagious diseases in humans. Experimentally infected non-human primates are used as animal models for studies of the pathogenesis of human measles. We established a reverse genetics system based on a highly pathogenic wild-type MV. Infection of monkeys with recombinant MV strains generated by reverse genetics enabled analysis of the molecular basis of MV pathogenesis. The essential *in vivo* function of accessory genes was indicated by infecting monkeys with recombinant MV strains deficient in the expression of accessory genes. Furthermore, recombinant wild-type MV strains expressing enhanced green fluorescent protein enabled visual tracking of MV-infected cells *in vitro* and *in vivo*. To date, three different molecules have been identified as receptors for MV. Signaling lymphocyte activation molecule (SLAM, also called CD150), expressed on immune cells, is a major receptor for MV. CD46, ubiquitously expressed in all nucleated cells in humans and monkeys, is a receptor for vaccine and laboratory-adapted strains of MV. The newly identified nectin-4 (also called poliovirus-receptor-like-4) is an epithelial cell receptor for MV. However, recent findings have indicated that CD46 acts as an MV receptor *in vitro* but not *in vivo*. The impact of the receptor usage of MV *in vivo* on the disease outcome is now under investigation.

Keywords: measles virus, monkey, pathogenesis, tropism, reverse genetics, receptor, EGFP

INTRODUCTION

Measles is a febrile disease that typically occurs in small children; the incubation period is 10–14 days, after which clinical symptoms such as fever, coughing, and a characteristic rash appears. Since measles is accompanied by immunosuppression, it has a high frequency of complication with secondary bacterial infections, such as otitis media or pneumonia. Although developed countries are eradicating measles by promoting effective vaccination, measles remains an important issue, especially in developing countries (Griffin, 2007).

Measles virus (MV), belonging to the genus *Morbillivirus* of the family Paramyxoviridae, is an enveloped virus with a non-segmented negative strand RNA genome. The MV genome has six genes that encode the nucleocapsid (N), phospho (P), matrix (M), fusion (F), hemagglutinin (H), and large (L) proteins (**Figure 1A**). MV contains two envelope glycoproteins: the H protein, which is responsible for receptor binding and is important for determining cell tropism of MV; and the F protein, which mediates membrane fusion (Navaratnarajah et al., 2009). The P gene encodes the P protein and the non-structural V and C proteins. The V and C proteins are important for antagonizing the host interferon (IFN) response (Gerlier and Valentin, 2009).

To date, three different molecules have been identified as receptors for MV. Signaling lymphocyte activation molecule (SLAM, also called CD150), expressed in certain immune system cells including activated B and T lymphocytes, mature dendritic cells, and macrophages, is a receptor for wild-type MV and vaccine and laboratory-adapted strains of MV (Tatsuo et al., 2000). CD46 (also called membrane cofactor protein), expressed in all human and monkey nucleated cells, is a receptor for vaccine and laboratory-adapted strains of MV (Dorig et al., 1993; Naniche et al., 1993). Recently, nectin-4 [also called poliovirus-receptor-like-4 (PVRL4)] has been identified as the epithelial receptor for wild-type MV (Muhlebach et al., 2011; Noyce et al., 2011).

Several animal models have been used for studying the pathogenesis of MV (Griffin, 2007). Cotton rats, rats, hamsters, mice, and ferrets can be infected with MV and are commonly used as small animal models for MV pathogenesis. After identification of CD46 and SLAM as MV receptors, numerous transgenic and knock-in mice expressing human CD46 and/or SLAM were established and intensively used to study different aspects of MV infection (Sellin and Horvat, 2009). However, non-human primates are the only animals that exhibit acute disease similar to that seen in humans. In this review, we discuss recent findings regarding tropism and pathogenesis of MV; these findings were obtained by infecting monkeys with recombinant wild-type MV.

HISTORICAL BACKGROUND OF MONKEY MODELS

When infected with measles, monkeys exhibit similar symptoms as seen in humans. This was reported as early as 1911, after inoculating monkeys with blood from measles patients (Anderson and Goldberger, 1911). In 1921, it was reported that measles could be transmitted from humans to monkeys by placing a filtered throat swab from a measles patient into the tracheae of monkeys (Blake and Trask, 1921a). These authors also performed histological analysis of infected monkeys (Blake and Trask, 1921b). However,

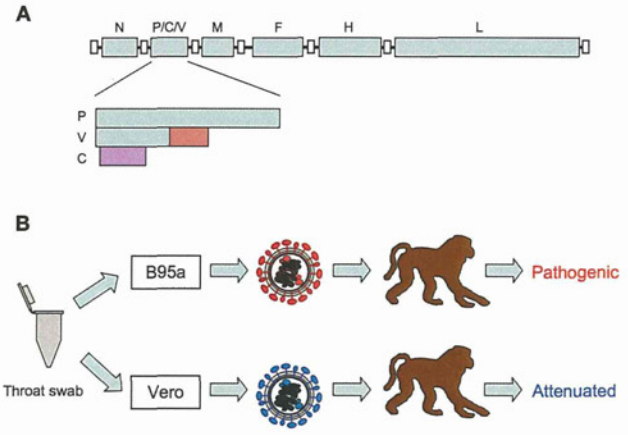

FIGURE 1 | (A) Schematic diagram of measles virus genome. The P gene encodes the P protein and the non-structural V and C proteins. The V protein is translated from an edited RNA with a non-templated G residue. The V protein-specific region is indicated in red. The C protein is translated from an alternative open reading frame (purple) initiated by the second AUG. **(B)** Isolation of wild-type MV using B95a cells. Pathogenic wild-type MV strains can be isolated by inoculating throat swabs from measles patients in B95a cells. MV strains isolated in Vero cells lose their pathogenicity.

at this time, "MV" had not yet been discovered. MV was first isolated in 1954 from a specimen obtained from a measles patient (Enders and Peebles, 1954). Enders and Peebles (1954) inoculated human and monkey cell cultures with a throat swab taken from a young boy named David Edmonston and isolated MV from these cultures. After this, it was discovered that MV isolated from normal human renal cells caused clinical signs similar to those of human measles in monkeys (Peebles et al., 1957). Since then, numerous studies have been carried out by infecting monkeys with MV, measles vaccines, or specimens from measles patients (Griffin, 2007). In such experiments, two species of monkeys, cynomolgus monkey (*Macaca fascicularis*) and rhesus monkey (*Macaca mulatta*), serve as good animal models. New World monkeys are more susceptible to MV than Old World monkeys, and infection of marmoset (*Saguinus mystax*) with MV results in a fulminant disease (Levy and Mirkovic, 1971; Albrecht et al., 1980).

In the past, it was well known that infection of monkeys with materials from measles patients induced clinical signs similar to those of human measles (Nii et al., 1964; Yamanouchi et al., 1970; Sakaguchi et al., 1986). However, curiously enough, infection of monkeys with MV isolated and propagated in cultured cells did not always induce these clinical signs (Enders et al., 1960; Yamanouchi et al., 1970; van Binnendijk et al., 1994). This riddle was solved by the introduction of B95a cells (a marmoset B-lymphoid cell line) for isolation and propagation of MV (Kobune et al., 1990). Kobune et al. (1990, 1996) found that MV strains could be efficiently isolated in B95a cells using materials from measles patients. More importantly, MV strains isolated from B95a cells retained their original pathogenicity in monkeys. These studies indicated that vaccine and laboratory-adapted strains of MV previously isolated from non-lymphoid cells such as Vero cells were not true MV (**Figure 1B**). A decade later, it was found that the MV receptor SLAM is highly expressed on B95a cells (Tatsuo et al., 2000), which accounts for the efficient isolation of pathogenic MV from patient samples. Similar to MV strains isolated from B95a cells, MV strains isolated and propagated in monkey mononuclear cells, human cord blood cells, human B lymphoblastoid cell lines, and Vero cells expressing SLAM replicated well in monkeys and induced clinical signs of measles (van Binnendijk et al., 1994; McChesney et al., 1997; Zhu et al., 1997; Auwaerter et al., 1999; El Mubarak et al., 2007; Bankamp et al., 2008). These results suggest that expression of SLAM on cells used for isolation is important for isolation of pathogenic MV.

REVERSE GENETICS OF MV

Reverse genetics refers to the methods used for recovering infectious viruses from the cDNA that encodes the viral genome. By using this method, mutations or extra transcription units can be introduced into viral genomes by the modification of cDNA plasmids. Reverse genetics of MV was first established based on the Edmonston vaccine strain (Radecke et al., 1995). However, as previously mentioned, viruses derived from the Edmonston vaccine strain do not induce clinical symptoms of measles in monkeys. Therefore, reverse genetics of pathogenic wild-type MV was needed for the study of MV pathogenesis in monkeys. To this end, we first determined the complete nucleotide sequence of the genome of the pathogenic wild-type IC-B strain (NC_001498/AB016162; Takeuchi et al., 2000), which was isolated in Tokyo in 1984 by using B95a cells (Kobune et al., 1990). Then, we constructed a complete cDNA plasmid of the IC-B strain named p(+)MV323, and successfully recovered infectious MV (IC323 strain) from the p(+)MV323 plasmid (Takeda et al., 2000). Importantly, the IC323 strain induced clinical signs such as rash, Koplik's spots, and lymphopenia similar to human measles in infected monkeys, indicating that the IC323 strain retains the original pathogenicity of the IC-B strain. Now, infectious MV strains can be easily recovered from cDNA plasmids by using an improved protocol (Takeda et al., 2005).

Reverse genetics of other wild-type MV strains has been reported for the HL strain isolated in Japan (Terao-Muro et al., 2008) and the KS strain isolated in Sudan (Lemon et al., 2011). For vaccine strains of MV, reverse genetics for the Schwarz/Moraten vaccine strain (Combredet et al., 2003; del Valle et al., 2007) and the AIK-C vaccine strain (Nakayama et al., 2001) have also been reported. Reverse genetics for vaccine strains are being used as a platform to generate new multivalent vaccines expressing antigens of other pathogens (Billeter et al., 2009) and oncolytic viruses for cancer therapy (Russell and Peng, 2009).

FUNCTION OF MV ACCESSORY PROTEINS *IN VIVO*

The P gene of MV encodes two non-structural proteins, namely the C and V proteins. However, the function of the C and V proteins *in vivo* was not well understood. The C protein is a small (186 amino acid), highly positively charged protein. To study the function of the C protein in the context of the natural course of MV pathogenesis, we generated an IC323 strain deficient in the expression of the C protein, wtMV(C−), by using the reverse genetics of wild-type MV (Takeuchi et al., 2005). Notably, the growth of wtMV(C−) in cynomolgus monkeys was dramatically reduced

when compared to the IC323 strain. A similar growth defect of the IC323 strain deficient in the expression of the C protein, C^{ko}, *in vivo* was observed in rhesus monkeys (Devaux et al., 2008). Interestingly, C^{ko} induced more inflammatory cytokines such as tumor necrosis factor alpha (TNF)-α and interleukin (IL)-6 and interferon (IFN)-α and -β in infected monkeys.

The V protein is translated from an edited mRNA of the P gene (Griffin, 2007). Thus, the amino-terminal domain of the V protein has the same amino acid sequence as the P protein, and the carboxyl-terminal domain of the V protein has a highly conserved amino acid sequence forming a zinc-binding domain, which is important for function as an interferon antagonist (Gerlier and Valentin, 2009). An IC323 strain deficient in the expression of the V protein, V^{ko}, was generated by introducing nucleotide mutations in the RNA-editing signal in the P gene (Devaux et al., 2008). The growth of V^{ko} in infected rhesus monkeys was lower than that of the parental IC323 strain. V^{ko} induced more inflammatory cytokines (TNF-α and IL-6) and IFN-α and -β. An IC323 strain unable to antagonize STAT1 function, STAT1-blind virus, was generated by introducing three amino acid substitutions in the shared domain of the P and V proteins (Devaux et al., 2011). The STAT1-blind virus induced short-lived viremia and no clinical signs in infected rhesus monkeys. This virus induced more inflammatory cytokines (TNF-α and IL-6) and a Th1/Th2 balance cytokine (IL-12) in infected monkeys. Taken together, these findings indicate that the C and V proteins are not non-essential gene products as previously thought, but are stringently required for antagonizing host innate immune and inflammatory responses *in vivo*.

In contrast, *in vitro* studies indicated that the V protein blocks IFN-α/β signal transductions in infected cells, inhibits TLR7-mediated IFN-α production in human plasmacytoid dendritic cells, and inhibits IFN induction in infected cells by interacting with MDA5 (Gerlier and Valentin, 2009). Furthermore, the C protein appears to inhibit IFN induction in infected cells by regulating viral RNA synthesis (Nakatsu et al., 2008). Thus, it is necessary to elucidate whether the *in vivo* phenotypes of C- and V-deficient viruses are similar to the *in vitro* phenotypes.

MV TROPISM *IN VIVO*

Recent advances in the study of virus tropism have included the introduction of enhanced green fluorescent protein (EGFP)-expressing viruses. *In vivo* tropism of *Morbillivirus* can be visualized with high sensitivity in living animals as well as tissue samples by using EGFP-expressing recombinant canine distemper viruses (von Messling et al., 2004). Similarly, MV target tissues or organs can be visualized with high sensitivity by infecting cynomolgus monkeys with an EGFP-expressing IC323 strain (**Figure 2**). de Swart et al. (2007) infected rhesus and cynomolgus monkeys with an IC323 strain expressing EGFP (Hashimoto et al., 2002) and examined the tropism of wild-type MV *in vivo*. They indicated that the major target cells of wild-type MV were B and T lymphocytes and CD11c-positive, major histocompatibility complex (MHC) class-II-positive dendritic cells. This result is consistent with the fact that SLAM is a receptor for wild-type MV. Infection of ciliated epithelial cells in the trachea and lungs was also detected, suggesting the presence of another receptor for MV in epithelial cells.

Regarding the early target cells of wild-type MV, classical textbooks describe that the primary targets of MV are the epithelial cells of the respiratory tract. However, SLAM is not expressed in these epithelial cells. To examine the early target cells of wild-type and vaccine strains of MV in the lung, de Vries et al. (2010) infected cynomolgus monkeys with EGFP-expressing IC323 or vaccine strains of MV via the intratracheal or aerosol route. They found

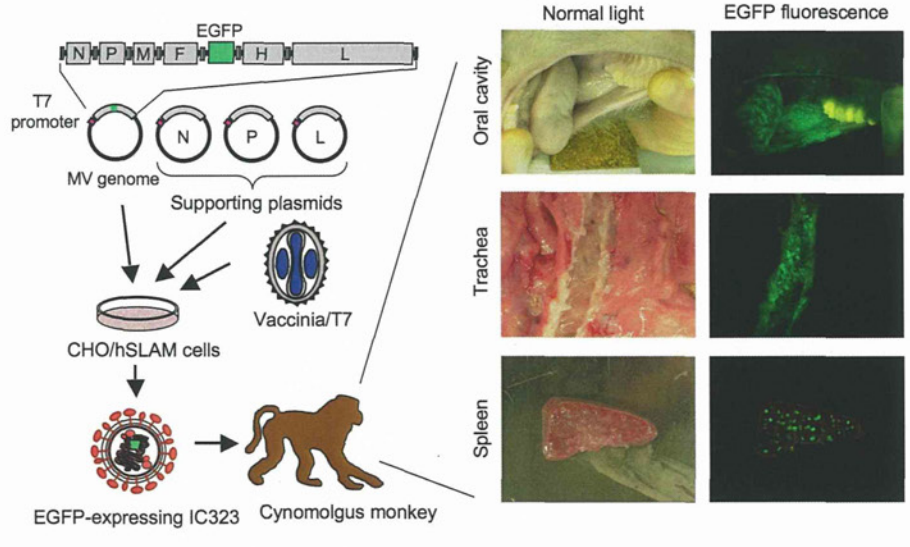

FIGURE 2 | Schematic diagram of reverse genetics of wild-type MV expressing EGFP and infection of monkeys. A plasmid carrying the full-genome cDNA of the IC-B strain and the EGFP gene under the control of the T7 promoter is introduced into CHO cells expressing human SLAM (CHO/hSLAM), along with three supporting plasmids expressing N, P, and L proteins, respectively, under the control of the T7 promoter. After infection with vaccinia virus expressing the T7 RNA polymerase, wild-type MV expressing EGFP can be recovered by mixing with B95a cells. EGFP fluorescence in tissues and organs of infected monkeys can be detected using a fluorescence microscope.

that CD11c-positive cells, which include alveolar macrophages and dendritic cells, were the major targets of both viruses. Interestingly, although viral replication and cellular tropism in the lungs were similar for the two viruses, only wild-type MV caused significant viremia, suggesting a growth defect of the vaccine strain in lymphocyte cells. Similarly, to examine the early target cells of wild-type MV, Lemon et al. (2011) infected cynomolgus monkeys with an EGFP-expressing wild-type MV based on the KS strain by aerosol infection and found that the early target cells of wild-type MV in monkeys are macrophages and dendritic cells. These studies indicated that alveolar macrophages and dendritic cells but not the epithelial cells of the respiratory tract are the early target cells of wild-type MV.

Nectin-4 is a newly identified epithelial cell receptor (EpR) for MV. To examine the effect of nectin-4-using activity of MV on disease outcomes in monkeys, an IC323 strain recognizing SLAM but not nectin-4 was generated by introducing amino acid mutations in the H protein (Leonard et al., 2008). At that time, nectin-4 had not been identified as a MV receptor, and this strain was called EpR-blind virus. When rhesus monkeys were infected with EpR-blind virus via the conjunctiva and nares, this virus induced viremia and clinical signs in infected monkeys but did not propagate in the lungs. This result indicates the importance of nectin-4 for the propagation of MV in the lungs, which is required for the subsequent exit of MV from the host. Inversely, to examine the impact of the recognition of SLAM by MV, an IC323 strain recognizing nectin-4 but not SLAM, SLAM-blind, was generated (Leonard et al., 2010). When rhesus monkeys were infected with the SLAM-blind virus, it elicited no clinical symptoms. This result indicates that SLAM recognition is necessary for MV virulence and pathogenesis.

Vaccine and laboratory-adapted strains of MV can utilize both CD46 and SLAM as cellular receptors. However, surprisingly, the impact of the CD46-using activity of vaccine and laboratory-adapted strains of MV on their tissue and organ tropism and attenuation is not well understood. As CD46 is ubiquitously expressed on all nucleated human and monkey cells, vaccine, and laboratory-adapted strains of MV may infect all tissues and organs of humans and monkeys. If so, this tropism shift may have great consequences on vaccine attenuation. In this context, de Vries et al. (2010) indicated that only CD11c-positive cells were infected with the EGFP-expressing vaccine strain via the aerosol route, suggesting that vaccine strains do not use CD46 *in vivo*. However, when the replication of vaccine and laboratory-adapted strains of MV in monkeys is limited, it will be difficult to identify infected cells in tissues. Furthermore, the infection of vaccine and laboratory-adapted strains of MV may be restricted because of mutations in the P/C/V genes, which are important for antagonizing the host IFN response (Gerlier and Valentin, 2009). Therefore, the tropism shift that solely occurs via the H protein should be evaluated using the wild-type MV expressing EGFP, which bears the H protein of a vaccine strain, such as the IC/EdH strain we developed previously (Takeuchi et al., 2002).

We recently infected cynomolgus monkeys with EGFP-expressing wild-type or IC/EdH strains and found that SLAM-expressing lymphocytes were the main targets of both strains, indicating that CD46 does not act as a receptor for vaccine and laboratory-adapted strains of MV *in vivo* (**Figure 3**; Takeuchi et al., 2012). One possible explanation for the limited expansion of the EGFP-expressing IC/EdH strain *in vivo* is the activation status of lymphocytes. It is known that stimulated lymphocytes are efficiently infected with MV and that stimulated lymphocytes express SLAM (Tatsuo et al., 2000). Thus, lymphocytes expressing SLAM may appear to be infected with both strains. The EGFP-expressing IC/EdH strain that entered into quiescent lymphocytes via the CD46 may not grow well in those cells. Alternatively, the expression level of CD46 *in vivo* may be too low to allow MV dissemination by cell–cell fusion, as it was reported that high CD46 density is required for MV-induced cell–cell fusion (Anderson et al., 2004). For whatever the reason, the growth of the EGFP-expressing IC/EdH strain was less efficient than that of the EGFP-expressing wild-type strain (Takeuchi et al., 2012), suggesting that the CD46-recognition ability of vaccine and laboratory-adapted MV strains plays a role in the MV attenuation. Further studies are required to elucidate the relationship between CD46-recognition ability and MV attenuation.

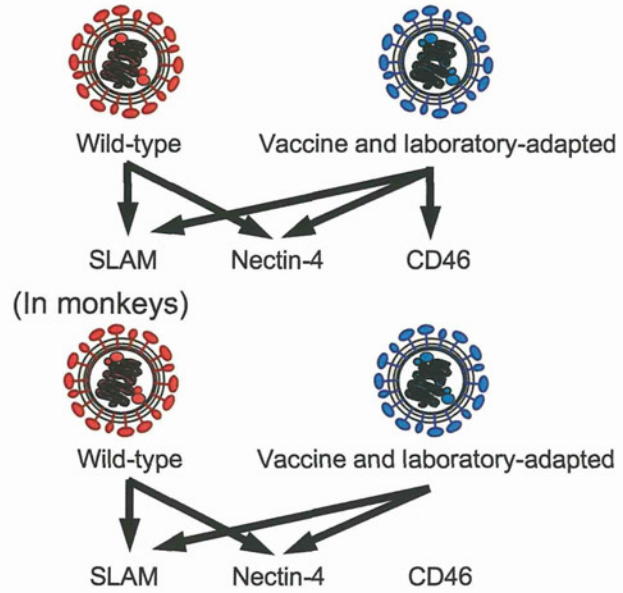

FIGURE 3 | Receptor usage of the wild-type and vaccine and laboratory-adapted strains of MV. Nectin-4 is a recently identified epithelial cell receptor for MV.

CONCLUSION

As described in this review, our IC323 strain, recovered from a plasmid carrying the full-genome cDNA of the IC-B strain, is now used as a standard wild-type MV strain in MV research. Furthermore, EGFP-expressing IC323 strains are ideal tools for the study of tissue and organ tropism of wild-type MV *in vivo*. Although the use of monkeys has several limitations, monkey models still provide the only reliable animal model for the study of the pathogenesis of MV in humans. The combination of wild-type and vaccine

MV strains generated by reverse genetics and monkey models will provide new insights into the relationship between viral gene functions or individual mutation(s) and the pathogenesis of MV.

ACKNOWLEDGMENTS

This paper was supported by a grant-in-aid (No. 23659227) from the Ministry of Education, Culture, Sports, Science, and Technology of Japan.

REFERENCES

Albrecht, P., Lorenz, D., Klutch, M. J., Vickers, J. H., and Ennis, F. A. (1980). Fatal measles infection in marmosets pathogenesis and prophylaxis. *Infect. Immun.* 27, 969–978.

Anderson, B. D., Nakamura, T., Russell, S. J., and Peng, K.-W. (2004). High CD46 receptor density determines preferential killing of tumor cells by oncolytic measles virus. *Cancer Res.* 64, 4919–4926.

Anderson, J. F., and Goldberger, J. (1911). Experimental measles in the monkey: a supplemental note. *Public Health Rep.* 26, 887–895.

Auwaerter, P. G., Rota, P. A., Elkins, W. R., Adams, R. J., DeLozier, T., Shi, Y., Bellini, W. J., Murphy, B. R., and Griffin, D. E. (1999). Measles virus infection in rhesus macaques: altered immune responses and comparison of the virulence of six different virus strains. *J. Infect. Dis.* 180, 950–958.

Bankamp, B., Hodge, G., McChesney, M. B., Bellini, W. J., and Rota, P. A. (2008). Genetic changes that affect the virulence of measles virus in a rhesus macaque model. *Virology* 373, 39–50.

Billeter, M. A., Naim, H. Y., and Udem, S. A. (2009). Reverse genetics of measles virus and resulting multivalent recombinant vaccines: applications of recombinant measles viruses. *Curr. Top. Microbiol. Immunol.* 329, 129–162.

Blake, F. G., and Trask, J. D. Jr. (1921a). Studies on measles. I. Susceptibility of monkeys to the virus of measles. *J. Exp. Med.* 33, 385–412.

Blake, F. G., and Trask, J. D. Jr. (1921b). Studies on measles. II. Symptomatology and pathology in monkeys experimentally infected. *J. Exp. Med.* 33, 413–422.

Combredet, C., Labrousse, V., Mollet, L., Lorin, C., Delebecque, F., Hurtrel, B., McClure, H., Feinberg, M. B., Brahic, M., and Tangy, F. (2003). A molecularly cloned Schwarz strain of measles virus vaccine induces strong immune responses in macaques and transgenic mice. *J. Virol.* 77, 11546–11554.

de Swart, R. L., Ludlow, M., de Witte, L., Yanagi, Y., van Amerongen, G., McQuaid, S., Yuksel, S., Geijtenbeek, T. B. H., Duprex, W. P., and Osterhaus, A. D. M. E. (2007). Predominant infection of CD150+ lymphocytes and dendritic cells during measles virus infection of macaques. *PLoS Pathog.* 3, e178. doi:10.1371/journal.ppat.0030178

de Vries, R. D., Lemon, K., Ludlow, M., McQuaid, S., Yuksel, S., van Amerongen, G., Rennick, L. J., Rima, B. K., Osterhaus, A. D. M. E., de Swart, R. L., and Duprex, W. P. (2010). In vitro tropism of attenuated and pathogenic measles virus expressing green fluorescent protein in macaques. *J. Virol.* 84, 4714–4724.

del Valle, J. R., Devaux, P., Hodge, G., Wegner, N. J., McChesney, M. B., and Catteneo, R. (2007). A vectored measles virus induces hepatitis B surface antigen antibodies while protecting macaques against measles virus challenge. *J. Virol.* 81, 10597–10605.

Devaux, P., Hodge, G., McChesney, M. B., and Cattaneo, R. (2008). Attenuation of V- or C-defective measles viruses: infection control by the inflammatory and interferon responses of rhesus monkeys. *J. Virol.* 82, 5359–5367.

Devaux, P., Hudacek, A. W., Hodge, G., Valle, J. R., McChesney, M. B., and Cattaneo, R. (2011). A recombinant measles virus unable to antagonize STAT1 function cannot control inflammation and is attenuated in rhesus monkeys. *J. Virol.* 85, 348–356.

Dorig, R. E., Marcil, A., Chopra, A., and Richardson, C. D. (1993). The human CD46 molecule is a receptor for measles virus (Edmonston strain). *Cell* 75, 295–305.

El Mubarak, H. S., Yuksel, S., van Amerongen, G., Mulder, P. G. H., Mukhtar, M. M., Osterhaus, A. D. M. E., and de Swart, R. L. (2007). Infection of cynomolgus macaques (*Macaca fascicularis*) and rhesus macaques (*Macaca mulatta*) with different wild-type measles viruses. *J. Gen. Virol.* 88, 2028–2034.

Enders, J. F., Katz, S. L., Milovanovic, M. V., and Holloway, A. (1960). Studies on an attenuated measles-virus vaccine I. Development and preparation of the vaccine: techniques for assay of effects of vaccination. *N. Engl. J. Med.* 263, 153–159.

Enders, J. F., and Peebles, T. C. (1954). Propagation in tissue cultures of cytopathic agents from patients with measles. *Proc. Soc. Exp. Biol. Med.* 86, 277–286.

Gerlier, D., and Valentin, H. (2009). Measles virus interaction with host cells and impact on innate immunity. *Curr. Top. Microbiol. Immunol.* 329, 163–191.

Griffin, D. E. (2007). "Measles virus," in *Fields Virology*, 5th Edn, eds D. M. Knipe, P. M. Howley, D. E. Griffin, R. A. Lamb, M. A. Martin, B. Roizman, and S. E. Straus (Philadelphia, PA: Lippincott Williams & Wilkins), 1551–1585.

Hashimoto, K., Ono, N., Tatsuo, H., Minagawa, H., Takeda, M., Takeuchi, K., and Yanagi, Y. (2002). SLAM (CD150)-independent measles virus entry as revealed by recombinant virus expressing green fluorescent protein. *J. Virol.* 76, 6743–6749.

Kobune, F., Sakata, H., and Sugiura, A. (1990). Marmoset lymphoblastoid cells as a sensitive host for isolation of measles virus. *J. Virol.* 64, 700–705.

Kobune, F., Takahashi, H., Terao, K., Ohkawa, T., Ami, Y., Suzaki, Y., Nagata, N., Sakata, H., Yamanouchi, K., and Kai, C. (1996). Nonhuman primate models of measles. *Lab. Anim. Sci.* 46, 315–320.

Lemon, K., de Vries, R. D., Mesman, A. W., McQuaid, S., van Amerongen, G., Yuksel, S., Ludlow, M., Rennick, L. J., Kuiken, T., Rima, B. K., Geijtenbeek, T. B. H., Osterhaus, A. D. M. E., Duprex, W. P., and de Swart, R. L. (2011). Early target cells of measles virus after aerosol infection of non-human primates. *PLoS Pathog.* 7, e1001263. doi:10.1371/journal.ppat.1001263

Leonard, V. H. J., Hodge, G., Valle, J. R., McChesney, M. B., and Cattaneo, R. (2010). Measles virus selectively blind to signaling lymphocytes activation molecule (SLAM; CD150) is attenuated and induces strong adaptive immune responses in rhesus monkeys. *J. Virol.* 84, 3413–3420.

Leonard, V. H. J., Sinn, P. L., Hodge, G., Miest, T., Devaux, P., Oezguen, N., Braun, W., McCray, P. B. Jr., McChesney, M. B., and Cattaneo, R. (2008). Measles virus blind to its epithelial cell receptor remains virulent in rhesus monkeys but cannot cross the airway epithelium and is not shed. *J. Clin. Invest.* 118, 2448–2458.

Levy, B. M., and Mirkovic, R. R. (1971). An epizootic of measles in a marmoset colony. *Lab. Anim. Sci.* 21, 33–39.

McChesney, M. B., Miller, C. J., Rota, P. A., Zhu, Y., Antipa, L., Lerche, N. W., Ahmed, R., and Bellini, W. J. (1997). Experimental measles. I. Pathogenesis in the normal and the immunized host. *Virology* 233, 74–84.

Muhlebach, M. D., Mateo, M., Sinn, P. L., Prufer, S., Uhlig, K. M., Leonard, V. H., Navaratnarajah, C. K., Frenzke, M., Wong, X. X., Sawatsky, B., Ramachandran, S., McCray, P. B. Jr., Cichutek, K., von Messling, V., Lopez, M., and Cattaneo, R. (2011). Adherens junction protein nectin-4 is the epithelial receptor for measles virus. *Nature* 480, 530–533.

Nakatsu, Y., Takeda, M., Ohno, S., Shirogane, Y., Iwasaki, M., and Yanagi, Y. (2008). Measles virus circumvents the host interferon response by different actions of the C and V proteins. *J. Virol.* 82, 8296–8306.

Nakayama, T., Komase, K., Uzuka, R., Hoshi, A., and Okafuji, T. (2001). Leucine at position 278 of the AIK-C measles virus vaccine strain fusion protein is responsible for reduced syncytium formation. *J. Gen. Virol.* 82, 2143–2150.

Naniche, D., Varior-Krishnan, G., Cervoni, F., Wild, T. F., Rossi, B., Rabourdin-Combe, C., and Gerlier, D. (1993). Human membrane cofactor protein (CD46) acts as a cellular receptor for measles virus. *J. Virol.* 67, 6025–6032.

Navaratnarajah, C. K., Leonard, V. H. J., and Cattaneo, R. (2009). Measles virus glycoprotein complex assembly, receptor attachment, and cell entry. *Curr. Top. Microbiol. Immunol.* 329, 59–76.

Nii, S., Kamahora, J., Mori, Y., Takahashi, M., Nishimura, S., and Okuno, Y. (1964). Experimental pathology of measles in monkeys. *Biken J.* 6, 271–297.

Noyce, R. S., Bondre, D. G., Ha, M. N., Lin, L. T., Sisson, G., Tsao, M. S., and Richardson, C. D. (2011). Tumor cell marker PVRL4 (nectin 4) is an epithelial cell receptor for measles virus. *PLoS Pathog.* 7, e1002240. doi:10.1371/journal.ppat.1002240

Peebles, T. C., McCarthy, K., Enders, J. F., and Holloway, A. (1957). Behavior of monkeys after inoculation of virus derived from patients with measles and propagated in tissue culture together with observations on spontaneous infections of these animals by an agent exhibiting similar antigenic properties. *J. Immunol.* 78, 63–74.

Radecke, F., Spielhofer, P., Schneider, H., Kaelin, K., Huber, M., Dotsch, C., Christiansen, G., and Billeter, M. A. (1995). Rescue of measles virus from cloned DNA. *EMBO J.* 14, 5773–5784.

Russell, S. J., and Peng, K. W. (2009). Measles virus for cancer therapy. *Curr. Top. Microbiol. Immunol.* 330, 213–241.

Sakaguchi, M., Yoshikawa, Y., Yamanouchi, K., Sata, T., Nagashima, K., and Takeda, K. (1986). Growth of measles virus in epithelial and lymphoid tissues of cynomolgus monkeys. *Microbiol. Immunol.* 30, 1067–1073.

Sellin, C. I., and Horvat, B. (2009). Current animal models: transgenic animal models for study of measles pathogenesis. *Curr. Top. Microbiol. Immunol.* 330, 111–127.

Takeda, M., Ohno, S., Seki, F., Hashimoto, K., Miyajima, N., Takeuchi, K., and Yanagi, Y. (2005). Efficient rescue of measles virus from cloned cDNA using SLAM-expressing Chinese hamster ovary cells. *Virus Res.* 108, 161–165.

Takeda, M., Takeuchi, K., Miyajima, N., Kobune, F., Ami, Y., Nagata, N., Suzaki, Y., Nagai, Y., and Tashiro, M. (2000). Recovery of pathogenic measles virus from cloned cDNA. *J. Virol.* 74, 6643–6647.

Takeuchi, K., Miyajima, N., Kobune, F., and Tashiro, M. (2000). Comparative nucleotide sequence analyses of the entire genomes of B95a cell-isolated and Vero cell-isolated measles viruses from the same patient. *Virus Genes* 20, 253–257.

Takeuchi, K., Nagata, N., Kato, S., Ami, Y., Suzaki, Y., Suzuki, T., Sato, Y., Tsunetsugu-Yokota, Y., Mori, K., Nguyen, V. N., Kimura, H., and Nagata, K. (2012). Wild-type measles virus with the hemagglutinin protein of the Edmonston vaccine strain retains wild-type tropism in macaques. *J. Virol.* PMID: 22238320. [Epub ahead of print].

Takeuchi, K., Takeda, M., Miyajima, N., Ami, Y., Nagata, N., Suzaki, Y., Shahnewaz, J., Kadota, S., and Nagata, K. (2005). Stringent requirement for the C protein of wild-type measles virus for growth in vitro and in macaques. *J. Virol.* 79, 7838–7844.

Takeuchi, K., Takeda, M., Miyajima, N., Kobune, F., Tanabayashi, K., and Tashiro, M. (2002). Recombinant wild-type and Edmonston strain measles viruses bearing heterologous H proteins: role of H protein in cell fusion and host cell specificity. *J. Virol.* 76, 4891–4900.

Tatsuo, H., Ono, N., Tanaka, K., and Yanagi, Y. (2000). SLAM (CDw150) is a cellular receptor for measles virus. *Nature* 406, 893–897.

Terao-Muro, Y., Yoneda, M., Seki, T., Watanabe, A., Tsukiyama-Kohara, K., Fujita, K., and Kai, C. (2008). Heparin-like glycosaminoglycans prevent the infection of measles virus in SLAM-negative cell lines. *Antiviral Res.* 80, 370–376.

van Binnendijk, R. S., van der Heijden, R. W., van Amerongen, G., UytdeHaag, F. G., and Osterhaus, A. D. (1994). Viral replication and development of specific immunity in macaques after infection with different measles virus strains. *J. Infect. Dis.* 170, 443–448.

von Messling, V., Milosevic, D., and Cattaneo, R. (2004). Tropism illuminated: lymphocyte-based pathways blazed by lethal morbillivirus through the host immune system. *Proc. Natl. Acad. Sci. U.S.A.* 101, 14216–14221.

Yamanouchi, K., Egashira, Y., Uchida, N., Kodama, H., Kobune, F., Hayami, M., Fukuda, A., and Shishido, A. (1970). Giant cell formation in lymphoid tissue of monkeys inoculated with various strains of measles virus. *Jpn. J. Med. Sci. Biol.* 23, 131–145.

Zhu, Y., Heath, J., Collins, J., Greene, T., Antipa, L., Rota, P., Bellini, W., and McChesney, M. (1997). Experimental measles. II. Infection and immunity in the rhesus macaque. *Virology* 233, 85–92.

Conflict of Interest Statement: The authors declare that the research was conducted in the absence of any commercial or financial relationships that could be construed as a potential conflict of interest.

Received: 30 November 2011; accepted: 09 January 2012; published online: 30 January 2012.

Citation: Kato S-i, Nagata K and Takeuchi K (2012) Cell tropism and pathogenesis of measles virus in monkeys. Front. Microbio. ***3****:14. doi: 10.3389/fmicb.2012.00014*

This article was submitted to Frontiers in Virology, a specialty of Frontiers in Microbiology.

Published online 22 February 2012

Nucleic Acids Research, 2012, Vol. 40, No. 11 ***4861–4878***
doi:10.1093/nar/gks162

Function of homo- and hetero-oligomers of human nucleoplasmin/nucleophosmin family proteins NPM1, NPM2 and NPM3 during sperm chromatin remodeling

Mitsuru Okuwaki[1,2,3,*], Ayako Sumi[1], Miharu Hisaoka[1], Ai Saotome-Nakamura[1,2], Satoko Akashi[4], Yoshifumi Nishimura[4] and Kyosuke Nagata[1]

[1]Faculty of Medicine and Graduate School of Comprehensive Human Sciences, [2]Initiative for the Promotion of Young Scientists' Independent Research, University of Tsukuba, 1–1–1 Tennodai, Tsukuba 305–8577, [3]PRESTO, Japan Science and Technology Agency, 4–1–8 Honcho, Kawaguchi 322–0012 and [4]Graduate School of Nanobioscience, Yokohama City University, 1-7-29 Suehiro-cho, Tsurumi-ku, Yokohama 230-0045, Japan

Received September 3, 2011; Accepted January 28, 2012

ABSTRACT

Sperm chromatin remodeling after oocyte entry is the essential step that initiates embryogenesis. This reaction involves the removal of sperm-specific basic proteins and chromatin assembly with histones. In mammals, three nucleoplasmin/nucleophosmin (NPM) family proteins–NPM1, NPM2 and NPM3–expressed in oocytes are presumed to cooperatively regulate sperm chromatin remodeling. We characterized the sperm chromatin decondensation and nucleosome assembly activities of three human NPM proteins. NPM1 and NPM2 mediated nucleosome assembly independently of other NPM proteins, whereas the function of NPM3 was largely dependent on formation of a complex with NPM1. Maximal sperm chromatin remodeling activity of NPM2 required the inhibition of its non-specific nucleic acid-binding activity by phosphorylation. Furthermore, the oligomer formation with NPM1 elicited NPM3 nucleosome assembly and sperm chromatin decondensation activity. NPM3 also suppressed the RNA-binding activity of NPM1, which enhanced the nucleoplasm–nucleolus shuttling of NPM1 in somatic cell nuclei. Our results proposed a novel mechanism whereby three NPM proteins cooperatively regulate chromatin disassembly and assembly in the early embryo and in somatic cells.

INTRODUCTION

Chromatin structure is significantly modified during spermatogenesis, resulting in the generation of highly condensed sperm chromatin. The core histones, H2A, H2B, H3 and H4, are largely removed and replaced with sperm-specific basic polypeptide protamines to form tight toroidal complexes. Sperm chromatin is rapidly reorganized in the oocytes after fertilization. During this process, protamines are efficiently removed and the canonical chromatin components, histones are deposited to form chromatin that can participate in zygote formation. This process is mediated by factor(s) present in the oocyte cytoplasm. In *Xenopus*, protamine removal and histone deposition are both mediated by an oocyte-specific acidic protein, nucleoplasmin, originally identified as a factor involved in chromatin assembly in *Xenopus* egg extracts (1,2). Huge amounts of histones are stored in *Xenopus* oocytes to ensure that DNA replication-coupled chromatin assembly occurs after fertilization and that subsequent cell division occurs without *de novo* transcription. Other important roles of nucleoplasmin during early embryogenesis include neutralization of the basic charge of histones and inhibition of their non-specific binding to DNA. Treatment of mouse embryonic carcinoma cell line F9 with nucleoplasmin induces the expression of oocyte-specific genes, suggesting that nucleoplasmin has a role in nuclear reprogramming by regulating global chromatin structure (3). Furthermore, ectopic expression of human NPM2, an ortholog of nucleoplasmin, in 293T cells induces the expression of pluripotency-associated genes (4). In mouse, the expression of NPM2 is restricted

*To whom correspondence should be addressed. Tel: +81 29 853 7950; Fax: +81 29 853 5983; Email: mokuwaki@md.tsukuba.ac.jp

in growing oocytes (5). Targeted disruption of the mouse NPM2 gene results in abnormal nuclear structure formation in oocytes and early embryonic cells, despite its dispensable function in sperm chromatin decondensation (5). Therefore, NPM2 plays an important role in the regulation of chromatin structure during early embryogenesis. Other family proteins, including NPM1 and NPM3, may play compensatory roles in NPM2-knockout mouse eggs. Human NPM1/nucleophosmin/B23 also has a potential role in sperm chromatin decondensation (6), both NPM1 and NPM3 are expressed in mouse oocytes (5), and inhibition of NPM3 expression using an antisense oligonucleotide prevents sperm chromatin remodeling in mouse fertilized eggs (7). These observations suggest that NPM family proteins play important roles in sperm chromatin remodeling.

Proteins in the NPM family share a conserved N-terminal core domain containing eight-stranded β-sheets (8). Crystal structural analyses of the N-terminal domains of nucleoplasmin, *Drosophila* nucleoplasmin-like protein dNLP, *Xenopus* NO38/NPM1 and human NPM1 and NPM2, demonstrated that the core domain forms a pentameric ring, while two pentamers associate in a head-to-head fashion to form a decamer (9–13). Other features of this family are acidic stretches extending from the core domains, which are implicated in efficient histone chaperone activity (14). Unlike other NPM proteins, NPM1 has an RNA-binding domain that is required for efficient nucleolar localization at the C-terminal end (15). Proteins in the NPM family are likely to form hetero-oligomers because of the significant conservation found in the core domains.

We have been studying the molecular mechanism of adenovirus (Ad) chromatin assembly and disassembly. Ad DNA is complexed with viral basic core proteins, V, VII and Mu, in the mature virions to produce the highly condensed Ad chromatin structure. Upon entry into host cell nuclei, Ad chromatin is decondensed after a change in the mode of interaction between the core proteins and DNA, and DNA is used as a template for early gene expression (16). Ad chromatin does not function as a template for replication and transcription *in vitro* because of its condensed structure, indicating that Ad chromatin remodeling is crucial for the initiation of transcription and replication. We previously identified host factors, Template Activating Factor-I (TAF-I) and NPM1/Nucleophosmin/B23 as host factors involved in Ad chromatin remodeling (17,18). TAF-I and NPM1 directly associate with viral basic core proteins to remodel the viral chromatin structure (16,19). Since the major core protein VII is an arginine-rich basic polypeptide and shows limited sequence similarity to sperm-specific basic proteins (20), adenovirus chromatin remodeling is an advantageous model system to understand sperm chromatin remodeling. Consistent with this, we previously demonstrated that both TAF-I and NPM1 have potential sperm chromatin decondensation activity as they mediate adenovirus chromatin remodeling (6,21).

The three NPM proteins are expressed in oocytes and eggs, so that NPM proteins may share overlapping roles due to the formation of hetero-oligomers via the conserved core domain. However, the oligomerization status and biochemical activities of the three human NPM proteins have yet to be established. This report characterized the sperm chromatin decondensation and nucleosome assembly activities of homo- and hetero-oligomers of the three human NPM proteins.

MATERIALS AND METHODS

Plasmids

Plasmids for NPM1 expression were previously described (6,18,22). Human and mouse NPM3 genes were cloned by PCR using cDNA prepared from HeLa cells and NIH3T3 cells by using oligonucleotide sets, 5′-aaaacgcgtcatatggcc gccggtactgcagc-3′ and 5′-aaaggatccctagggcctgccccctg ct-3′, and 5′-agctagcatatgttcagcatggcggccggcgc-3′ and 5′-a gctggatcctaaggcctgcccctgtgct-3′, respectively. The cDNA was digested with Nde I and Bam HI, and subcloned into the same sites of pET14b (Novagene). To add N-terminal Flag-tag, the cDNA cut out from pET14b-NPM3 by Nde I and Hind III was subcloned into the same sites of pBS-Flag vector. To construct pGEX6P1-NPM3 and pEGFPC1-Flag-NPM3, the cDNA was cut out from pBS-Flag-NPM3 by digestion with Bam HI and subcloned into the same sites of pGEX6P1 (GE Healthcare) or pEGFPC1 (Clonetech). The expression of His-tagged NPM3 was not successful in *Escherichia coli* using pET14b-NPM3, so the full length NPM3 cDNA was synthesized to optimize the sequence for the *E. coli* expression system. The optimized NPM3 sequence was subcloned into the Nde I and Bam HI sites of pET14b. Similarly, the human NPM2 cDNA optimized for expression in *E. coli* was synthesized and subcloned into the Nde I and Bam HI sites of pET14b. The NPM2 cDNA was cut out from pET14b vector by Nde I and Hind III, and subcloned into the same sites of pBS-Flag vector. Then, the Flag-tagged NPM2 cDNA was cut out by Bam HI digestion and subcloned into the Bam HI sites of pGEX6P1 and pEGFPC1 vectors. The sequences of synthesized cDNAs (Operon Biotechnologies) for human NPM2 and NPM3 will be provided upon request. For construction of the chimeric NPM1–3Ch protein, cDNAs for NPM1(1–120) and NPM3(146–178) were independently amplified using primer sets 5′-cacttagtagctgt ttccgaagaagaatct-3′ and T7 terminator primer, and 5′-ttctt cggaaacagctactaagtgctgtcc-3′ and T7 promoter primer, respectively, and appropriate pET14b vectors as templates. These two fragments were used as templates for second PCR using T7 promoter and terminator primers to amplify the full length cDNA. The cDNA was subcloned into the Nde I- and Bam HI-digested pET14b. To purify the NPM1–NPM3 complex, the cDNA for NPM3 containing N-terminal His-tag was cut out from pET14b-NPM3 vector by Nco I and Bam HI, and subcloned into the same sites of pETDuet-1 vector (Novagene). The NPM1 cDNA amplified by PCR with 5′- AGCGGATCCCATGGAAGATTCGATGGA CAT-3′ and T7 terminator primer, and pET14b-NPM1 as template was digested with Bam HI and subcloned into the Bgl II site of pETDuet-1 vector containing the

NPM3 cDNA. To construct phosphomimetic NPM2 proteins, oligonucleotide sets 5′-GCAGACGTTCGCGA TAAAGACCCAGTCAAGAAA-3′ and 5′-TGGGTCTT TATCGCGAACGTCTGCACGGATTTC-3′ for NPM2 S196D, and 5′-GAGCAGGCTCCGGTGAAACAGGT G-3′ and 5′-CACCGGAGCCTGCTCTTCCAGACT-3′ for S159D, and 5′-ATGCAGCATATGAACCTGGACG ACGCTGACGACGACGAAGAAAAAGCGGTTACT-3′ for 5D were used for PCR. NPM2 2D and 7D mutants were constructed using appropriate primer sets described above. The mutant cDNA was amplified by PCR and digested with Nde I and Bam HI, and subcloned into the same sites of pET14b.

Cell culture

HeLa cells and HEK293T cells were maintained in DMEM containing 10% FBS. HeLa cell lines expressing either EGFP–Flag (EF)–NPM1 or EF–NPM3 were established by transfection of pEGFPC1–Flag–NPM1 or pEGFP–Flag–NPM3 vectors. Cells stably expressing EGFP-tagged proteins were selected by 50 mg/l of G418. The colonies were isolated and the expression of EGFP-tagged proteins was examined by fluorescence microscope and western blotting with anti-Flag antibody.

Mouse oocytes and sperms preparation

MII-stage oocytes were prepared from the oviducts of 8-weeks-old ICR mice (SLC Japan, Inc.) supraovulated with equine chronic gonadotropin and human chronic gonadotropin. MII oocytes were separated from cumulus cells by hyaluronidase, and MII oocytes and cumulus cells were separately collected and used for western blotting. Sperms were isolated from testis of 12–14-weeks-old B6 mice. Sperms were washed with nuclei wash buffer (40 mM HEPES–KOH pH 7.2, 250 mM sucrose, 75 mM KCl, 0.5 mM spermidine and 0.15 mM spermine), permeabilized with the same buffer containing 0.33 mg/ml L-α-palmitoyl-lysophosphatidylcholine (SIGMA), 0.1% Nonidet P-40 and 10 mM dithiothreitol on ice for 10 min. The cells were washed with nuclei wash buffer, suspended in the same buffer containing 50% glycerol at a concentration of 1×10^5 nuclei/μl, frozen in liquid N_2, and kept at −80°C until use.

Protein purification, chemical cross linking experiments, limited trypsin digestion

Recombinant proteins were expressed in *E. coli* and purified as described previously (18). His-tagged NPM proteins were separated by SDS–PAGE and recovered from the gel. The proteins were eluted, precipitated with acetone and denatured in 6 M Guanidine–HCl containing 50 mM Tris–HCl pH 7.9, and 10 mM DTT. Denatured proteins were dialyzed in 50 mM Tris–HCl pH 7.9, 12.5 mM $MgCl_2$, 50 mM KCl, 0.5% NP-40 and 20% Glycerol for 3 h, and then the dialysis buffer was changed to buffer H (20 mM HEPES–NaOH pH 7.9, 50 mM NaCl, 0.5 mM EDTA, 10% Glycerol and 0.5 mM PMSF) and dialyzed for 6 h.

To purify the His–NPM3–NPM1 complex, extracts were prepared from *E. coli* BL21 strain transformed with pETDuet-NPM3/NPM1 vector. The complex was purified with His select Nickel Affinity Gel (Sigma Aldrich) according to the manufacturers' instruction. The eluted His–NPM3/NPM1 complex was then loaded on to a Mono Q column (0.1 ml, GE Healthcare) and purified with salt gradient from 0.1 to 0.6 M NaCl. The peak fraction containing both NPM1 and NPM3 was dialyzed as above. The samples (10 μg of NPM1 in 20 μl) were then separated by Superose 6 PC 3.2/30 column chromatography at a flow rate of 30 μl/min. Fractions (50 μl each) were collected and proteins were analyzed by SDS–PAGE and western blotting. Gel Filtration Calibration Kits (GE Healthcare) were used as molecular weight standards.

Phosphorylation of His-tagged NPM2 was performed with total cell extracts prepared from asynchronous and mitotic HeLa cells. Synchronization of HeLa cells and extracts preparation were performed as described previously (23). His–NPM2 (40 μg) was incubated with cell extracts (50 μg of proteins) at 37°C for 1 h in 20 mM Tris–HCl pH 7.9, 50 mM NaCl, 10 mM $MgCl_2$, 10% glycerol, 1 mM PMSF, 1 mM ATP and phosphatase inhibitors (10 mM β-D-glycerophosphate, 1 mM NaF and 1 mM Na_3VO_4). Then, His–NPM2 protein was purified with His select Nickel Affinity Gel as described above. The purified proteins were dialyzed in buffer H containing phosphatase inhibitors.

Chemical crosslinking experiments were performed with glutaraldehyde (Sigma). The proteins in buffer H were mixed with 0.05% glutaraldehyde and incubated at room temperature for 10 min. The reaction was terminated by adding SDS-sample loading buffer and boiling at 95°C for 10 min. The samples were separated by SDS–PAGE followed by silver staining or western blotting.

Blue Native (BN)–PAGE was performed with Native PAGE™ Novex Bis–Tris Gel System (Invitrogen) according to the manufacturers' instruction. Native Mark™ Unstained Protein Standard (Invitrogen) was used as molecular weight markers for BN–PAGE.

For trypsin digestion assay, recombinant proteins (500 ng) in buffer H were mixed with Trypsin (Sigma) and incubated at 37°C for 5 min. The reaction was stopped by adding SDS-sample loading buffer and boiled at 95°C for 5 min. Proteins were separated by 15% SDS–PAGE and visualized by Coomassie Brilliant Blue (CBB) staining or western blotting.

NCP assembly and DNA-binding assays

Nucleosome core particle (NCP) assembly assays were performed using 147-bp DNA fragment containing 5S rRNA gene sequence and core histones prepared as described previously (24). For DNA-binding assays shown in Figure 4, 196-bp DNA fragment was mixed with recombinant NPM2 proteins in 20 mM Tris–HCl pH 7.9, 100 mM NaCl, 10% Glycerol, 0.1 mg/ml of BSA. The complexes were loaded on 6% PAGE in 0.5 × TBE and the DNA was visualized with GelRed (Biotium) staining. Supercoiling assays were performed as described previously (6) using pCAGGS vector.

Sperm chromatin decondensation

Mouse sperm nuclei were isolated as above and sperm nuclei decondensation assays were performed as described previously (21). A total of 2×10^4 sperm nuclei were incubated with NPM proteins and incubated at 37°C. Sperm DNA stained with 4′,6-diamidino-2-phenylindole (DAPI) was observed under fluorescence microscope equipped with a color, cooled CCD camera (DP71, Olympus). Sperm size was measured by Image J software (http://rsb.info.nih.gov/ij/).

Antibodies

Anti-NPM3 serum was generated in rabbits using the GST–Flag–NPM3 protein as an antigen. Anti-NPM3 antibody was purified with His–NPM3-immobilized HiTrap NHS-activated HP column (GE Healthcare). Purified anti-NPM3 antibody does not cross react with other NPM proteins (data not shown). Anti-Flag (M2, Sigma), anti-His-tag (HIS1, Sigma) and anti-NPM1 (Invitrogene) were commercially available. Anti-PCNA and anti-mouse NPM2 antibodies are generous gifts from Dr A. Verreault and Dr M. Matzuk, respectively.

Cell extracts preparation and immunoprecipitation

Exponentially growing HeLa cells were disrupted in gentle sonication in buffer A (50 mM Tris–HCl pH 7.9, 0.1% Triton X-100 and 0.5 mM PMSF) containing 150 mM NaCl. The extracts were recovered by centrifugation with 15 000 rpm for 15 min and mixed with anti-NPM1 or anti-NPM3 antibody, and incubated at 4°C for 2 h. As a control, normal rabbit IgG (Santacruz Biotechnology) was used. The NPM proteins were recovered by the addition of protein A sepharose (GE Healthcare). Proteins were separated on 12.5% SDS–PAGE and analyzed by western blotting.

For immunoprecipitation of EGFP–Flag (EF) tagged NPM proteins, EF, EF–NPM1, EF–NPM2 and EF–NPM3 were transiently transfected to HeLa cells with Gene Juice (Novagene). Twenty four hours after transfection, the cell extracts were prepared as above and immunoprecipitation was performed with anti-Flag M2 agarose beads (Sigma). The proteins bound to the beads were washed extensively by buffer A containing 150 mM NaCl, and eluted with the same buffer containing Flag peptide (Sigma). The proteins were separated by SDS–PAGE and analyzed by western blotting.

Glycerol density gradient assay

Nuclear extracts (50 µl) prepared from HeLa cells were loaded on 15–35% glycerol density gradient in 20 mM HEPES–NaOH pH 7.9, 50 mM NaCl and 0.5 mM EDTA (2.1 ml). The samples were centrifuged at 35 000 rpm for 14 h at 4°C in S55S rotor (Hitachi Koki). Fractions (100 µl) were collected from the top and analyzed by SDS–PAGE and western blotting.

Immunofluorescence and FRAP analysis

To examine the localization of endogenous NPM1 and NPM3, HeLa cells grown on cover slips were fixed with 3% paraformardehyde and permeabilized in PBS containing 0.5% Triton X-100. Cells were then incubated with anti-NPM1 and NPM3 antibodies diluted with PBS containing 0.5% non-fat dry milk. Localization of proteins was visualized with secondary antibodies conjugating with AlexaFluor dyes (Molecular Probes). During final wash with PBS containing 0.1% Triton X-100, To-Pro-3 DNA staining dye (Molecular Probes) was added and incubated for 15 min at room temperature. Localization of proteins and DNA was observed under confocal microscope (LSM EXCITER; Carl Zeiss Microimaging, Inc.).

HeLa cells stably expressing EF–NPM1 or EF–NPM3 were subjected to FRAP analyses. Cells were grown on 35-mm glass base dishes (IWAKI). The dish was set on an inverted microscope (LSM EXCITER; Carl Zeiss Microimaging, Inc.) in an air chamber containing 5% CO_2 at 37°C, and the mobility of EGFP–tagged NPM proteins was analyzed by photobleaching with a Plan-Apochromat 63×/1.4 oil objective. EGFP signal in small nucleoli was bleached using 85% transmission of a 488-nm Ar laser (50 iterations), and images were collected (512 × 512 pixels, zoom 4.1, scan speed 13, pinhole 1 airy unit, LP505 emission filter and 1.0% transmission of a 488-nm Ar laser with 0.7% output power) every 0.5 s. The fluorescence intensity of the bleached area was measured using ZEN2008 software (Carl Zeiss Microimaging, Inc.). Background intensity was first subtracted from all the intensities measured and relative fluorescence intensity (RFI) was calculated as following: $RFI = (Ia/Ia0) \times (Ib0/Ib)$, where Ia is the fluorescence intensity of bleached area at each time points, Ia0 is the initial fluorescence intensity of bleached area, Ib is the fluorescence intensity of non-bleached nucleoli at each time point, and Ib0 is the initial fluorescence intensity of non-bleached nucleoli. Recovery curves were fit to a single exponential using the FRAP analysis module of the ZEN software (Carl Zeiss Microimaging, Inc.).

RESULTS

Association between NPM proteins in HeLa cells

We first examined the localization of human NPM proteins in HeLa cells. Enhanced green fluorescent protein (EGFP)-tagged NPM proteins were expressed in HeLa cells, and their localization was examined using fluorescent microscopy (Figure 1A). As previously reported (23,25,26), EF-tagged NPM1 and NPM3 preferentially localized in the nucleoli, whereas EF–NPM2 was distributed throughout the nucleus. The level of the EF–NPM3 signal was higher than that of NPM1 in both the nucleoplasm and cytoplasm. Furthermore, the expression pattern of endogenous NPM1 and NPM3 in HeLa cells was confirmed by immunofluorescence using specific antibodies (Figure 1B). Endogenous NPM1 and NPM3 were localized in the nucleolus: the staining patterns of NPM1 and NPM3 suggested that both are mainly found in the granular component of the nucleolus.

NPM1 and NPM3 are expressed ubiquitously. We then examined the interaction between endogenous NPM1 and NPM3 in cell extracts. Nuclear extracts prepared from

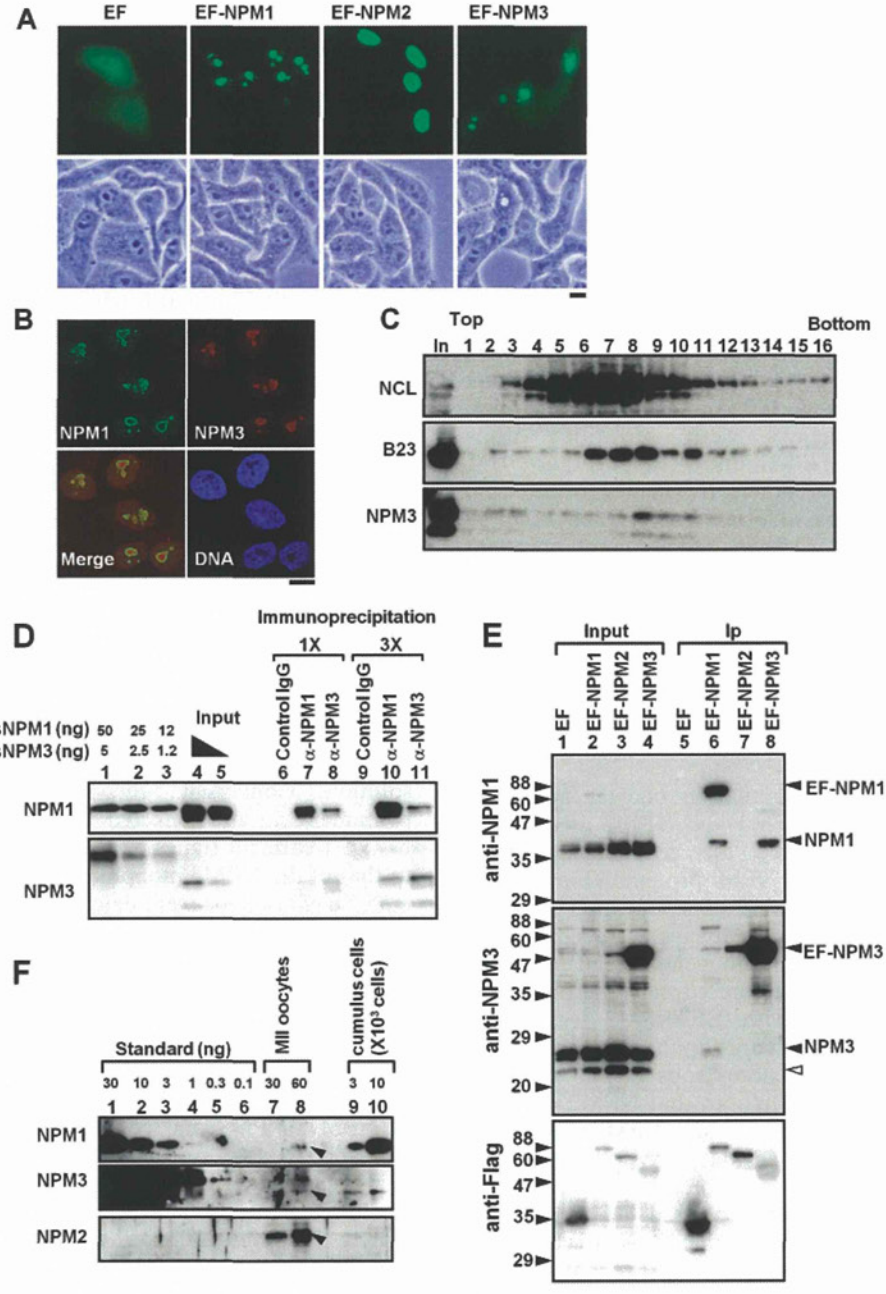

Figure 1. Association between human NPM proteins. (**A**) Localization of EGFP-tagged NPM proteins. EF, EF–NPM1, EF–NPM2 and EF–NPM3 were transiently expressed in HeLa cells and the localization of EGFP proteins was examined by fluorescent microscopy. Bottom panels are phase contrast images. Bar at the bottom indicates 10 μm. (**B**) Localization of endogenous NPM1 and NPM3 in HeLa cells. HeLa cells were subjected to immunofluorescence analysis using anti-NPM1 and anti-NPM3 antibodies. DNA was stained with TO-PRO-3. Images were observed under confocal microscopy. Bar at the bottom indicates 10 μm. (**C**) Glycerol density gradient of HeLa cell nuclear extracts. Nuclear extracts from HeLa cells were fractionated by 15–35% glycerol density gradient. Fractions collected from the top were analyzed by western blotting with anti-nucleolin (NCL), anti-B23 and anti-NPM3 antibodies. (**D**) Immunoprecipitation with anti-NPM proteins. HeLa cell extracts were subjected to immunoprecipitation with control Ig (lanes 6 and 9), anti-NPM1 (lanes 7 and 10), and anti-NPM3 (lanes 8 and 11) antibodies. Bound proteins were eluted with SDS-sample buffer (30 μl) and 3 (lanes 6–8) or 9 (lanes 9–11) μl of samples were separated on SDS–PAGE and analyzed by western blotting with anti-NPM1 and anti-NPM3 antibodies (top and bottom panels, respectively). As standard, recombinant His-NPM1 (50, 25, 12 ng for lanes 1–3) and His–NPM3 (5, 2.5, 1.2 ng for lanes 1–3), and increasing amounts of input extracts (lanes 4–5) were also loaded. (**E**) Immunoprecipitation of transiently expressed NPM proteins. EF, EF–NPM1, -NPM2 and -NPM3 were transiently expressed in HEK293T cells and cell extracts were prepared. Immunoprecipitation with anti-Flag antibody beads was performed. Input (lanes 1–4) and immunoprecipitated (lanes 5–8) proteins were analyzed by western blotting with anti-NPM1, -NPM3 and -Flag antibodies. Positions of NPM proteins are indicated at the right side of the panel. Blank arrow head shows the protein likely to be corresponded to NPM3 degradation product. (**F**) Expression level of NPM proteins in mouse MII oocytes. MII oocytes (30 and 60 cells for lanes 7 and 8, respectively) and cumulus cells (3×10^3 and 10×10^3 cells for lanes 9 and 10) were prepared from mice and analyzed by western blotting with anti-NPM1, -NPM3 and -NPM2 antibodies. Recombinant human NPM1 and mouse NPM3 were loaded on the same gel as standards (lanes 1–6). Positions of NPM proteins are indicated by arrow heads.

HeLa cells were fractionated using a 15–35% glycerol density gradient; fractions were collected from the top, the proteins in each fraction were analyzed by western blotting (Figure 1C). The NPM3 antibody generated in this study detected two NPM3 bands in the extracts (see the input lane of bottom panel). By comparing with the His-tagged recombinant protein (Figure 1D, lanes 1–5), the bottom band was likely to be a degradation product of full-length NPM3. Both NPM1 and NPM3 were broadly distributed and cofractionated in fractions 8–11. Since NPM1 and NPM3 (32.5 and 19 kDa, respectively) were recovered in higher molecular weight fractions than nucleolin (NCL, 76.6 kDa), both these proteins were mainly included in large protein complexes. To further test whether NPM1 and NPM3 formed a complex, immunoprecipitation assays were performed using antibodies specific for NPM1 and NPM3 (Figure 1D). Immunoprecipitation assays clearly demonstrated that NPM1 and NPM3 were associated with each other in extracts (lanes 6–11). Using recombinant proteins (migrating slower than endogenous proteins because of a His-tag) as standards (lanes 1–3), the amount of NPM3 (only full-length NPM3 (top band) was considered) in the input extracts derived from HeLa cells was rapidly estimated to be 1/10–1/20 of that of NPM1. Immunoprecipitation conducted using anti-NPM3 antibody indicated that NPM3 coprecipitated with higher amounts of NPM1 (lanes 8 and 11).

NPM2 expression is restricted in oocytes and early embryos (5), where both NPM1 and NPM3 are also expressed. We then examined the cellular interaction between NPM2 and other NPM proteins (Figure 1E). EF–tagged NPM proteins were expressed in HEK293T cells, and immunoprecipitation assays were conducted. EF–NPM1 coprecipitated endogenous NPM1 and NPM3 (lane 6). In contrast, the coprecipitation of endogenous NPM proteins with EF–NPM2 was barely detected (lane 7). EF–NPM3 coprecipitated with endogenous NPM1, but not with endogenous NPM3 (lane 8). These results raised the possibilities that NPM2 does not form a stable oligomer with other NPM proteins in oocytes and fertilized eggs and that NPM3 does not efficiently form a homo-oligomer in solution.

Three NPM proteins are expressed in mammalian oocytes (7), but their stoichiometry is unclear. To address this point, we examined the expression level of NPM proteins in mouse MII oocytes with specific antibodies using recombinant proteins as standards (Figure 1F). Because the anti-NPM1 antibody used in this study recognizes the C-terminal region (amino acids 259–294) of NPM1 and this region is completely identical in human and mouse NPM1, the amount of NPM1 in mouse MII oocytes was estimated using the human recombinant NPM1 protein as the standard. We used recombinant His-tagged mouse NPM3 as the standard for NPM3. The amounts of NPM1 and NPM3 were estimated to be ~1 ng/60 oocytes (0.51 fmol/oocyte, top panel lane 8) and 0.1 ng/60 oocytes (0.09 fmol/oocyte, middle panel lane 8), respectively. Consistent with the previous report (5), NPM2 was abundantly expressed in oocytes, and its expression level was much higher than that in cumulus cells (lanes 7–10). We could not precisely determine the expression level of NPM2 in mouse oocytes by using the mouse NPM2 antibody and recombinant human NPM2 proteins generated in this study because the similarity between mouse and human NPM2 is not sufficiently high (the two proteins are 65% identical). However, it was recently reported that the amount of NPM2 is ~75 pg (3.2 fmol)/oocyte (27). Taken together, these results support the idea that three NPM proteins are simultaneously expressed in oocytes and may play overlapping roles in sperm chromatin remodeling after fertilization.

Oligomerization of human NPM proteins

We next examined the oligomer formation ability of human NPM proteins. Bacterially expressed human NPM proteins were purified, and their oligomerization ability was tested using a chemical crosslinking assay (Figure 2A). NPM1 was subjected to SDS–PAGE and bands with 40 kDa and >200 kDa were detected even in the absence of chemical crosslinking (lane 1), indicating that NPM1 formed a stable oligomer. After glutaraldehyde (GA) treatment, ~200- and 160-kDa protein bands were observed for NPM1 and NPM2, respectively (lanes 2 and 4). In addition, bands >200 kDa were also detected. This result suggested that human NPM1 and NPM2 both formed stable pentamers and that some of the pentamers formed decamers in solution. Conversely, the band corresponding to a pentamer was not detected when NPM3 was subjected to GA treatment (lanes 5 and 6). Instead, a band similar to that of the NPM3 monomer and a minor population of a 55–60 kDa bands were detected. To further confirm the oligomerization status of NPM proteins, the proteins were analyzed by BN–PAGE (Figure 2B). BN–PAGE was originally developed for the separation of mitochondrial membrane proteins and has been used to determine the native mass and oligomeric status of proteins (28). By comparison with the molecular standards separated on the same gel (Figure 2B, right panel), the native masses of NPM1, NPM2 and NPM3 were estimated to be 358, 231 and 42 kDa, respectively. In parallel, gel filtration analysis revealed that His–NPM1 and His–NPM2 were fractionated at the positions corresponding to approximately 370 and 270 kDa, respectively (Figure 6D). In addition, we examined the mass of NPM3 by gel filtration, but it distributed broadly and we could not estimate native mass (data not shown). From these results and previous structural analyses (9–11,13), we concluded that both human NPM1 (34.7 kDa including the His-tag) and NPM2 (26.3 kDa including the His-tag) formed stable pentamers in solution and that two pentamers are assembled into decamers. On the other hand, NPM3 (21.5 kDa including the His-tag) is suggested to from dimers in solution. Consistent with this data, preliminary results from electrospray ionization mass spectrometry analyses suggested that NPM3 formed a dimer at low salt concentrations (data not shown). NPM1 and NPM2 treated with GA and separated by SDS–PAGE were mainly detected at around pentamer positions, while these proteins were suggested to form decamers by

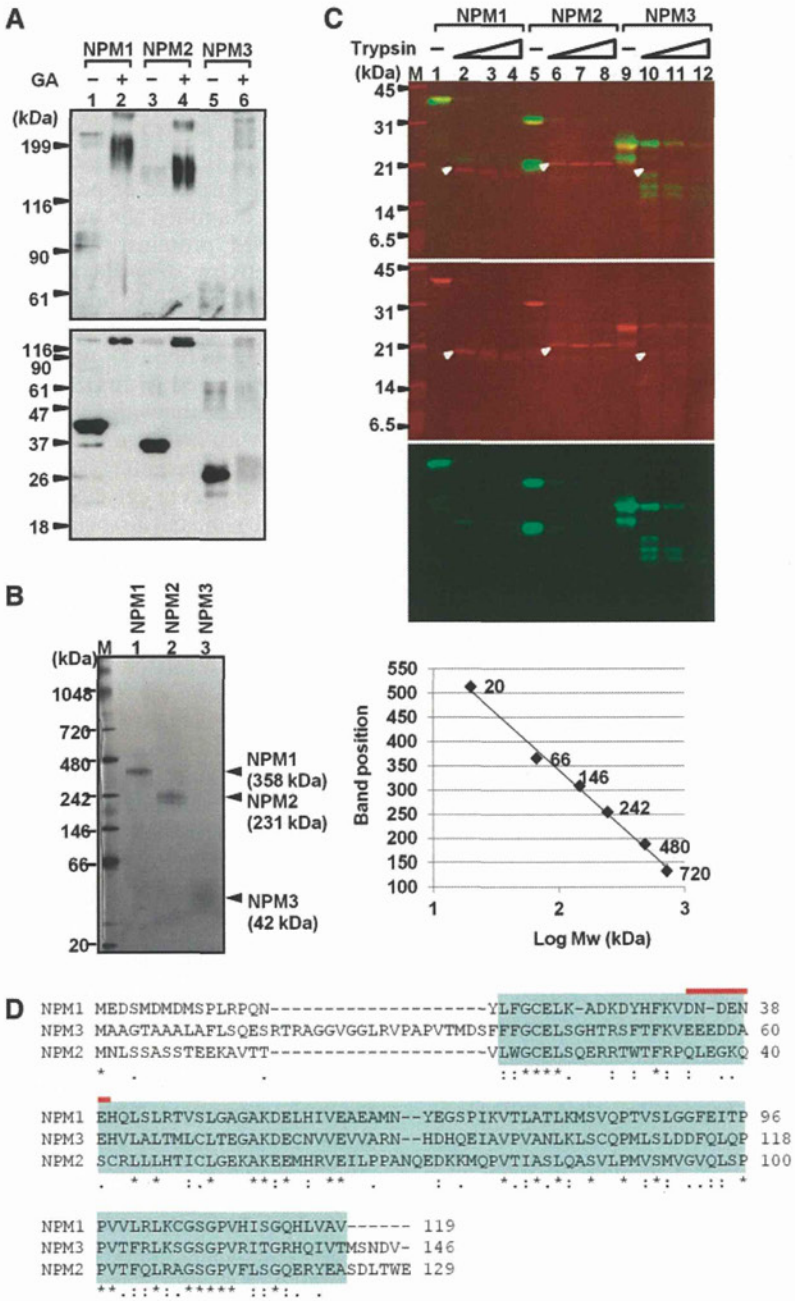

Figure 2. Oligomer formation of human NPM proteins. (**A**) Chemical crosslinking experiments. His-tagged NPM1, NPM2 and NPM3 (200 ng each) were treated without (lanes 1, 3 and 5) or with (lanes 2, 4 and 6) 0.05% glutaraldehyde (GA) and the fixed proteins were separated on 7.5% and 12.5% SDS–PAGE (top and bottom panels, respectively). Proteins were analyzed by western blotting with anti-His-tag antibody. Positions of molecular weight markers are indicated at the left side of the panels. (B) BN–PAGE analysis of NPM proteins. Recombinant His-tagged NPM1 (34.5 kDa), NPM2 (26.3 kDa) and NPM3 (21.5 kDa) (500 ng) were separated by 4–16% BN–PAGE and visualized with CBB staining. Lane M indicates molecular weight markers. The mobility of marker proteins was plotted as a function of their molecular weights (Mw) (right panel). The marker proteins were linearly separated and the masses of NPM proteins were estimated as shown at the right side of the gel. (**C**) Limited proteolysis of human NPM proteins. His-tagged NPM1, NPM2 and NPM3 were treated without or with increasing amounts of trypsin and incubated at 37°C for 5 min. Then the proteins were separated on 15% SDS–PAGE followed by CBB staining (Red) or western blotting with anti-His-tag antibody (Green). Positions of bands corresponding to the NPM core are indicated by arrow heads. CBB-stained gel and western blotting images are merged and shown in the top panel. (**D**) Alignment of the amino acid sequences of human NPM N-terminal domains. Amino acid sequences of human NPM1, NPM2 and NPM3 were aligned by ClastalW2 software (http://www.ebi.ac.uk/Tools/msa/clustalw2/) and conserved amino acids are highlighted by asterisks at the bottom of sequences. The conserved core domains of NPM proteins are indicated on blue background. The position of acidic 'A1 tract' is shown by red line at the top of the sequences.

BN–PAGE and gel filtration assays. This could be due to the assumption that the pentamer–pentamer interface is not efficiently crosslinked by GA, and two pentamers are dissociated under SDS–PAGE conditions.

The N-terminal regions of NPM family proteins are folded into a compact domain containing an eight-stranded β-barrel (sequences colored by light blue in Figure 2D). Unlike other NPM proteins, NPM3 does not form a stable pentamer. Therefore, we tested whether NPM3 is folded into a monomeric structure similar to that found in other NPM proteins by conducting a limited proteolysis assay using trypsin (Figure 2C). Full-length His-tagged NPM1, NPM2 and NPM3 were digested with increasing amounts of trypsin, and digested proteins were analyzed by SDS–PAGE followed by Coomassie Brilliant Blue (CBB) staining (colored with red) or western blotting using the anti-His-tag antibody (green). CBB-stained gels clearly showed the appearance of distinct protein bands of approximately 20 kDa corresponding to the core domain after the trypsin treatment of His-tagged NPM1 and NPM2 (lanes 1–8). Moreover, distinct bands of approximately 20 kDa were also detected when His–NPM3 was treated with trypsin (lanes 9–12). Western blotting with anti-His-tag antibody indicated that these peptides did not contain N-terminal ends. Based on these observations, it is strongly suggested that the N-terminal domain of NPM3 is folded into a typical NPM core structure. Trypsin treatment of NPM3 produced distinct bands <20 kDa, as detected by western blotting with anti-His-tag antibody, those of which were not apparent with NPM1 and NPM2 (lanes 10–12). Given the molecular weight and the positions of lysine and arginine residues of the NPM3 sequence from the N-terminal His-tag, these fragments were likely to correspond to fragments digested within the loop structures between the β-sheets (i.e. K76, R87 and K102, Figure 2D). These loop structures are known to be involved in the monomer–monomer interactions in the pentamer or in pentamer–pentamer interactions in the decamer (11,13). These results support the hypothesis that NPM3 is folded into a NPM core structure although the loop regions were susceptible to trypsin because of their lack of pentamer/decamer formation ability.

Sperm chromatin remodeling by human NPM proteins

Three NPM proteins are simultaneously expressed in oocytes (Figure 1F). Next, we examined whether NPM proteins may have sperm chromatin remodeling activity. Sperm chromatin remodeling consists of sperm chromatin decondensation by protamine removal and nucleosome assembly. Therefore, we examined both of these activities using NPM proteins *in vitro*. To examine the sperm chromatin remodeling activity of NPM proteins, mouse sperm nuclei were prepared and incubated in the absence or presence of NPM proteins. The size of DAPI-stained nuclei was measured by Image J software. As shown in Figure 3B, sperm nuclear size significantly increased in the presence of NPM1, but not in the presence of NPM2 or NPM3. This NPM1 activity depended on its concentration and incubation time (Figure 3C and D). Although mouse NPM2 was previously reported to induce mouse sperm chromatin decondensation by incubation for 24 h (27), we did not observe a significant increase in sperm size within 1 h. These results suggest that an additional factor is required for NPM2 and NPM3 to induce efficient protamine removal, including complex formation with other NPM family proteins or post-translational modifications.

We then examined the nucleosome assembly activity of human NPM proteins. We first examined the histone-binding activity of NPM proteins using GST-tagged human NPM proteins and core histones purified from HeLa cells (Figure 3E). GST alone did not precipitate histone proteins (lane 5), whereas four core histones efficiently precipitated with GST–NPM proteins (lanes 6–8). This indicated that all NPM proteins were similarly associated with histones under the assay conditions used. *Xenopus* nucleoplasmin (NPM2) is mainly associated with H2A–H2B dimers in egg extracts, but we observed that all NPMs were similarly associated with both histones H2A–H2B and H3–H4 *in vitro* (data not shown). We then sought to determine the nucleosome assembly activity of NPM proteins. Core histones were preincubated with increasing amounts of His-tagged NPM proteins (Figure 3A), mixed with a 147-bp DNA fragment, and incubated. The mixtures were separated by native polyacrylamide gel electrophoresis (Figure 3F). When histone alone was incubated with DNA, the DNA was present in large aggregates that could not enter the gel (lane 1). In contrast, when histones were preincubated with increasing amounts of NPM1, free DNA and NCP bands increased in a dose-dependent manner (lanes 2–6). The activity of NPM2 was also detected when its concentration was low, but DNA and NPC bands were decreased when NPM2 concentration was increased (lanes 7–11). This suggests that NPM2 randomly associates with DNA and/or DNA–histone complexes. When histones were preincubated with NPM3, DNA–histone aggregation decreased, and free DNA and NCP bands were clearly detected (lanes 12–16). To further verify the nucleosome assembly activity of NPM proteins, a supercoiling assay using relaxed plasmid DNA was conducted (Figure 3G). NPM1 mediated nucleosome assembly, and supercoil was introduced in plasmid DNA in a dose-dependent manner (lanes 2–4). In the presence of low concentration of NPM2 (lanes 5 and 6), supercoil was slightly introduced in plasmid DNA, and this weak activity was decreased in the presence of higher amounts of NPM2 (lane 7). In addition, we could not detect efficient nucleosome assembly activity of NPM3 (lanes 8–10) using supercoiling assay. Thus, we concluded that NPM3 binds to histones and inhibits DNA–histone aggregation, although this NPM3 activity is insufficient to form chromatin on long DNA as a histone chaperone. This is consistent with an earlier observation that the histone chaperone activity of NPM3 is significantly lower than that of NPM1 (29).

Effect of NPM2 phosphorylation on its sperm chromatin remodeling activity

We focused on the effect of post-translational modifications on NPM2 activity as a stimulatory mechanism for

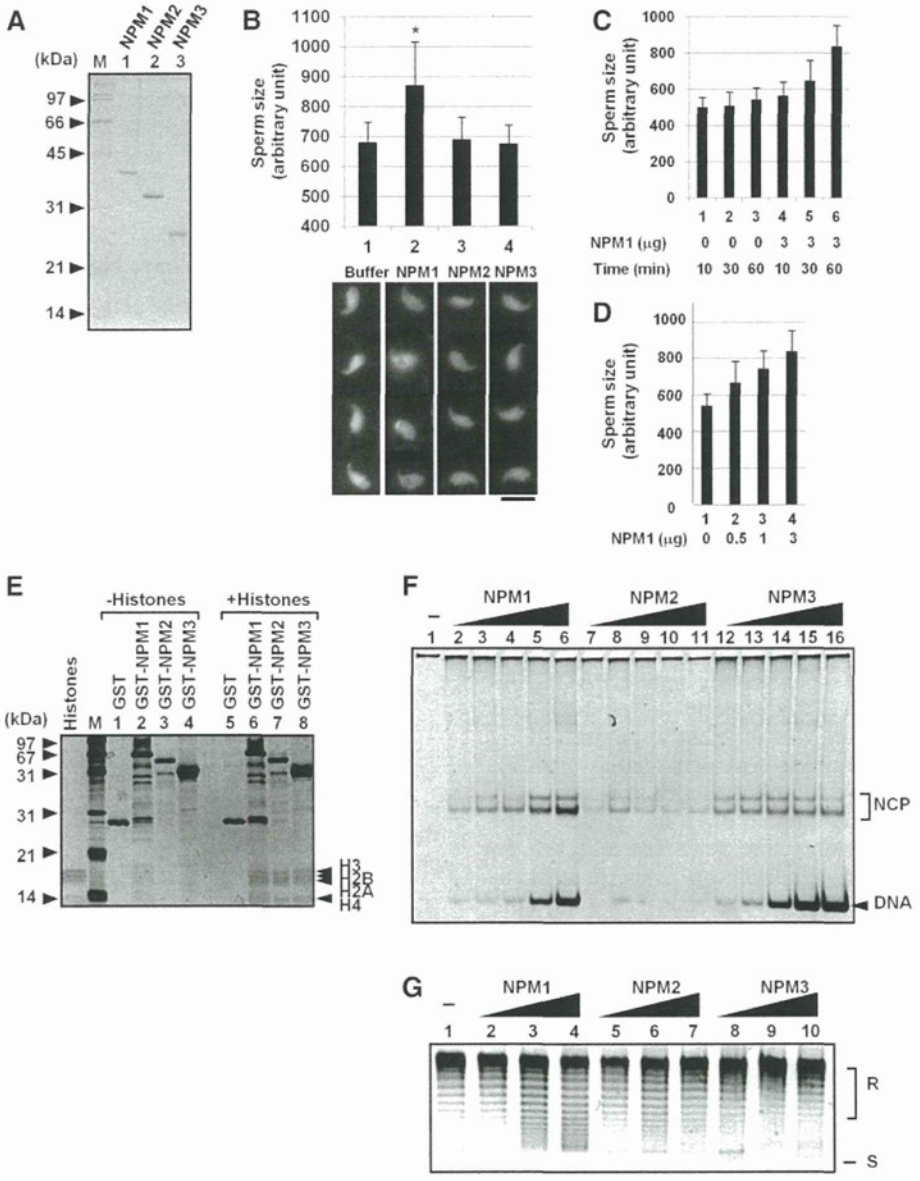

Figure 3. Sperm chromatin remodeling by human NPM proteins. (**A**) Purified proteins. His-tagged NPM proteins were expressed in *E. coli* and purified. Proteins (200 ng each) were separated by 12.5% SDS–PAGE and visualized with CBB staining. Positions of molecular weight markers are indicated at the left side of the panel. (**B**) Sperm chromatin decondensation by NPMs. Mouse sperm nuclei (1×10^5) were incubated for 60 min without or with 3 μg of purified NPM1, NPM2, or NPM3. Sperm nuclei were fixed with formardehyde and stained with DAPI. Bar at the bottom of the panels indicates 10 μm. Four typical sperm nuclei are shown for each sample. Size of the sperm nuclei ($n > 30$) were estimated by Image J software and averaged. Results are means ± SD and statistical *P*-values were calculated and indicated * for $P < 0.05$. (**C** and **D**) Sperm chromatin decondensation by NPM1. Sperm nuclei were incubated in the presence or absence of NPM1 and incubated for 10–60 min as indicated at the bottom of the graph (C) or for 60 min (D). Size of sperm nuclei was analyzed as in (B). (**E**) Histone-binding activity of human NPM proteins. GST, GST-tagged NPM1, NPM2, and NPM3 (1 μg each) were mixed without (lanes 1–4) or with core histones (1 μg, lanes 5–8) purified from HeLa cells in the buffer containing 150 mM NaCl. The mixtures were recovered by glutathione sepharose beads. The proteins were separated by 15% SDS–PAGE and visualized with silver staining. Positions of molecular weight markers and core histones are shown at the left and right side of the panel, respectively. (**F**) Histone transfer assay. Increasing amounts of His-tagged NPM1, NPM2 and NPM3 (lanes 2–6, 7–11 and 12–16, respectively) (50, 100, 200, 300 and 400 ng for each protein) were incubated with core histones (100 ng) and incubated. Then the 147-bp DNA fragment (30 ng) were added and further incubated at 37°C for 30 min. The mixtures were separated by 6% PAGE in 0.5× TBE. DNA was visualized by staining with GelRed. Positions of free DNA and nucleosome core particle (NCP) are indicated at the right side of the panel. (**G**) Supercoiling assay. His-tagged NPM1, NPM2 and NPM3 (100, 300, and 1000 ng for lanes 2–4, 5–7 and 8–10) were incubated with core histones (100 ng). Then plasmid DNA (100 ng) treated with topoisomerase I was added to NPM-histone mixture and incubated. Plasmid DNA was purified and analyzed by 1% agarose gel electrophoresis in 1× TBE and visualized with GelRed staining. Positions of relaxed (R) and supercoiled (S) DNA are indicated at the right side of the panel.

NPM2. The activity of *Xenopus* NPM2 was strictly regulated by phosphorylation during oogenesis and after fertilization (30). Mouse NPM2 is likely to be highly phosphorylated in metaphase II stage eggs and pronuclear stage zygotes (31). Thus, mammalian NPM2 function is also likely to be regulated by phosphorylation. Mitotic cell extracts prepared from HeLa cells and asynchronous HeLa cell extracts were used as kinase sources to mimic metaphase II stage eggs. A phosphorylated protein-specific dye, Pro-Q Diamond, was used to show that NPM2 proteins incubated with asynchronous and mitotic extracts were phosphorylated (Figure 4A, lanes 5 and 6). Based on the intensity of Pro-Q Diamond stained gel, NPM2 was most efficiently phosphorylated by mitotic extracts. This suggests that either kinases present in asynchronous and mitotic extracts differentially phosphorylated NPM2 or that the activity of a specific kinase in mitotic extracts was higher than that in asynchronous extracts. Because the histone transfer activity of recombinant NPM2 seemed to be inhibited by its non-specific DNA binding, we first examined the effect of NPM2 phosphorylation on its DNA-binding activity (Figure 4B). The 196-bp DNA fragment was incubated with increasing amounts of control or phosphorylated NPM2 proteins, and the complexes were separated by native PAGE. As expected, NPM2 bound DNA directly (lanes 2–5), and this DNA-binding activity was efficiently suppressed by phosphorylation with mitotic extracts (lanes 10–13). Next, we tried to identify the phosphorylation site(s) affecting NPM2 activity. Human NPM2 has typical cdc2 consensus serine residues at amino acids 159 and 196. In addition, N-terminal phosphorylation sites present in *Xenopus* nucleoplasmin/NPM2 are conserved in the human NPM2 protein. These sites were substituted by aspartic acid (D) to mimic phosphorylation status. NPM2 S159D, S196D, S159/196D (2D), 5D (S4, S5, S7, S8 and T9 were substituted by D) and 7D (combination of 2D and 5D) were incubated in the presence of interphase and mitotic extracts, and phosphorylation status was examined by Pro-Q Diamond staining (Figure 4C). NPM2 was efficiently phosphorylated by mitotic extracts (lane 2 and 9) and the phosphorylation was significantly reduced when two cdc2 consensus sites were substituted with D (lanes 10–12). N-terminal phosphorylation sites could be slightly phosphorylated by mitotic extracts (lanes 13 and 14), although these sites were not major phosphorylation sites in mitotic HeLa cell extracts. To examine the effect of phosphorylation of NPM2 on its activity, 2D, 5D and 7D mutants were tested for sperm chromatin decondensation activity (Figure 4D). Wild-type and 2D NPM2 proteins did not show significant sperm chromatin decondensation activity. In contrast, both 5D and 7D mutants slightly increased sperm nuclear size although the activity was lower than that of NPM1. The effect of NPM2 phosphorylation on its histone transfer activity was also examined (Figure 4E). NPM2 wild type did not efficiently transfer histones onto DNA fragments (lanes 1–5). The substitution of S159 and S196 with aspartic acids enhanced NCP formation (lanes 6–17). In addition, phosphomimetic mutation at the N-terminal region enhanced the NCP formation activity of NPM2 independently on S159 and S196 mutations (lanes 18–25). These results indicate that the phosphorylation of NPM2 at the N-terminal region plays a crucial role in sperm chromatin decondensation and chromatin assembly activities. Moreover, a kinase present in oocytes, but not in HeLa cells, and the cdc2 kinase are suggested to be required to fully activate the sperm chromatin remodeling activity of NPM2.

Oligomeric NPM3 may have histone chaperone activity

The low histone chaperone activity of NPM3 was presumably due to its lack of pentamer/decamer formation. To test this possibility, we constructed a chimeric protein in which the N-terminal core domain of NPM1 was fused with the C-terminal acidic region of NPM3 (NPM1–3Ch) (Figure 5A). SDS–PAGE clearly showed that both C-terminal truncated NPM1 (NPM1ΔC3) and NPM1–3Ch formed stable oligomers that could not be dissociated by SDS–PAGE sample buffer, and bands of approximately 100 and 70 kDa being detected in addition to monomer bands (lanes 3 and 4). Sperm nuclear size increased in the presence of NPM1, but not in the presence of NPM3 (Figure 5B). Sperm nuclear size increased and its structure was almost disrupted in the presence of the NPM1–3Ch protein. The supercoiling assay demonstrated that NPM3 and NPM1ΔC3 protein had a weak nucleosome assembly activity (Figure 5C, lanes 5–10). In contrast, the NPM1–3Ch protein showed a distinct nucleosome assembly activity (lanes 11–13). These results strongly suggest that the C-terminal region of NPM3 functions as a histone chaperone domain when it is included in the oligomer.

Effect of NPM3 on NPM1 function

NPM3 alone could not form homopentamers/decamers, but it was associated with NPM1 in cell extracts (Figure 1), suggesting that NPM3 formed a pentamer only with NPM1. To test this, purified NPM1 was mixed with increasing amounts of NPM3, denatured in guanidine hydrochloride and renatured by extensive dialysis. The oligomerization status of the renatured proteins was analyzed using a chemical crosslinking assay (Figure 6A). Proteins were separated by SDS–PAGE and visualized with silver staining and western blotting with an anti-NPM3 antibody (left and right panels, respectively). After GA treatment in the presence of NPM1, NPM3 was included in large complexes with molecular masses of approximately 180–200 kDa and >200 kDa (lanes 4, 6 and 8 in the right panel). The same proteins were also analyzed by BN–PAGE and visualized with silver staining (Figure 6B). NPM1 or NPM3 alone was detected at the position of approximately 350 kDa or 40 kDa, respectively (lanes 1 and 2). When the NPM1–NPM3 complexes were resolved by BN–PAGE, five main bands (bands 1–5 shown at the right side of the panel) were detected. The intensity of band 2 in addition to bands 4 and 5 increased when NPM3 ratio in the complex increased (lanes 3–5). The bands 4 and 5 corresponded to the NPM3 dimers and trimers that failed to associate with NPM1. The size of band 2 was estimated to be 310 kDa. i.e. similar to the size of the assembly of

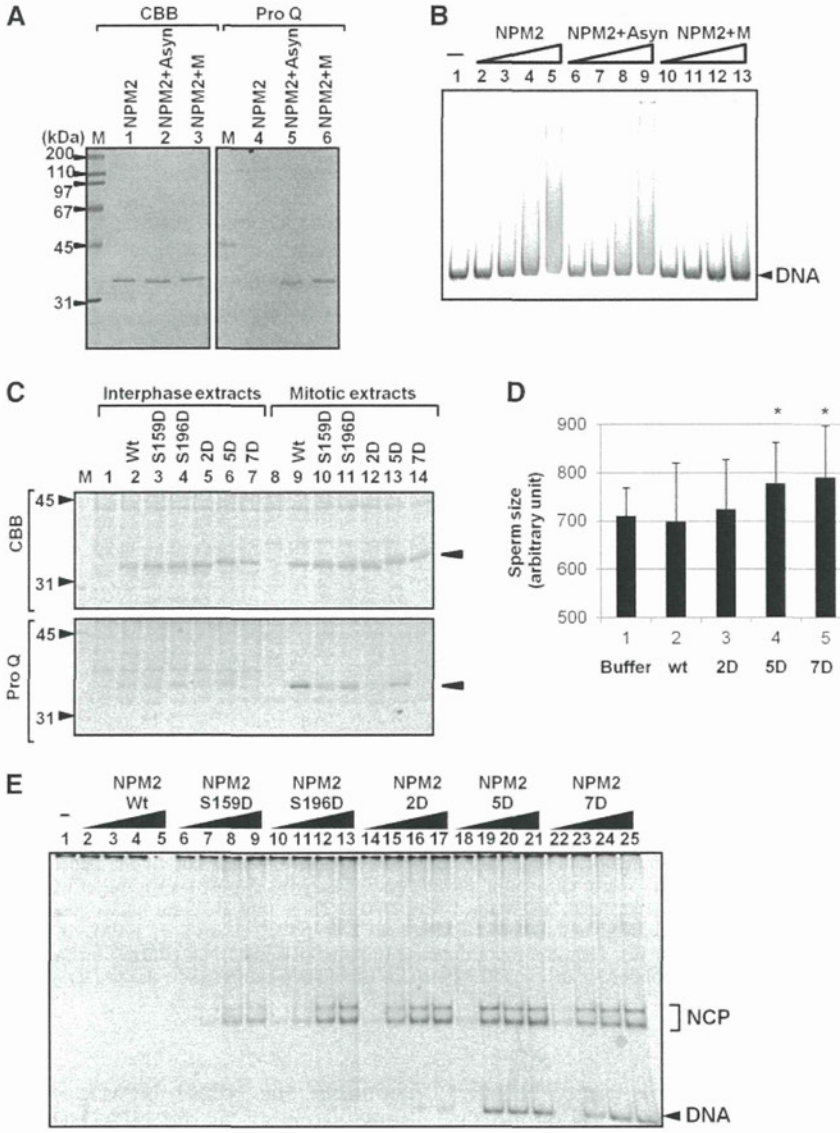

Figure 4. Effect of phosphorylation on NPM2 sperm chromatin remodeling activity. (**A**) Phosphorylation of recombinant NPM2. Purified His–NPM2 was mixed and incubated without or with asynchronous (+Asyn) or mitotic (+M) HeLa cell extracts followed by purification with the Ni-NTA resin. Dialyzed proteins (200 ng) were separated on 10% SDS–PAGE and visualized with CBB and Pro-Q Diamond staining (lanes 1–3 and 4–6, respectively). The 45-kDa marker protein (ovalbumin) was detected by Pro-Q Diamond staining. Positions of molecular weight markers are indicated at the left side of the panel. (**B**) DNA-binding activity of recombinant NPM2. The 196-bp DNA fragment (100 ng) were mixed with increasing amounts (100, 200, 400 and 800 ng for each protein) of control NPM2 (lanes 2–5) or NPM2 phosphorylated by asynchronous (lanes 6–9) or mitotic (lanes 10–13) extracts. The mixtures were analyzed by native PAGE in 0.5× TBE and DNA was visualized with GelRed staining. (**C**) Phosphorylation of NPM2 mutants by extracts. NPM2 wild type (wt), S159D, S196D, S159/196D (2D), 5D and 7D mutant proteins (500 ng) were incubated with asynchronous (lanes 1–7) or mitotic (lanes 8–14) cell extracts (5 μg of proteins) and SDS-sample buffer was added. Proteins were analyzed by SDS–PAGE and Pro-Q diamond or CBB staining (top and bottom panels, respectively). Positions of NPM2 proteins are indicated by arrow heads at the right side of the panels. (**D**) Sperm chromatin decondensation by NPM2 proteins. Mouse sperm nuclei were incubated in the absence or presence of NPM2 wt, 2D, 5D and 7D (3 μg) and the size of sperm nuclei ($n > 30$) were estimated by Image J software and averaged. Results are means ± SD and statistical *P*-values were calculated and indicated by asterisk for $P < 0.05$. (**E**) Histone transfer activity of phosphorylated NPM2. Histone transfer assay was performed as in Figure 3F with increasing amounts (100, 200, 300 and 400 ng for each protein) of NPM2 wt, S159D, S196D, 2D, 5D and 7D. The mixtures were separated on 6% PAGE in 0.5× TBE and DNA was visualized with GelRed staining. Positions of free DNA and NCP are indicated at the right side of the panel.

two His–NPM1 (34.5 kDa):His–NPM3 (21.5 kDa) (4:1) pentamers (319 kDa). These results suggest that NPM1 and NPM3 preferentially form pentamers at a ratio of 4:1, and two NPM1:NPM3 pentamers form a decamer in solution. However, it should be noted that the an oligomer with different stoichiometry was also detected on BN–PAGE (band 3). To further confirm oligomer formation between NPM1 and NPM3, His-tagged NPM3 and non-tagged NPM1 were coexpressed and purified with the Ni–NTA resin. Under this condition, all NPM1

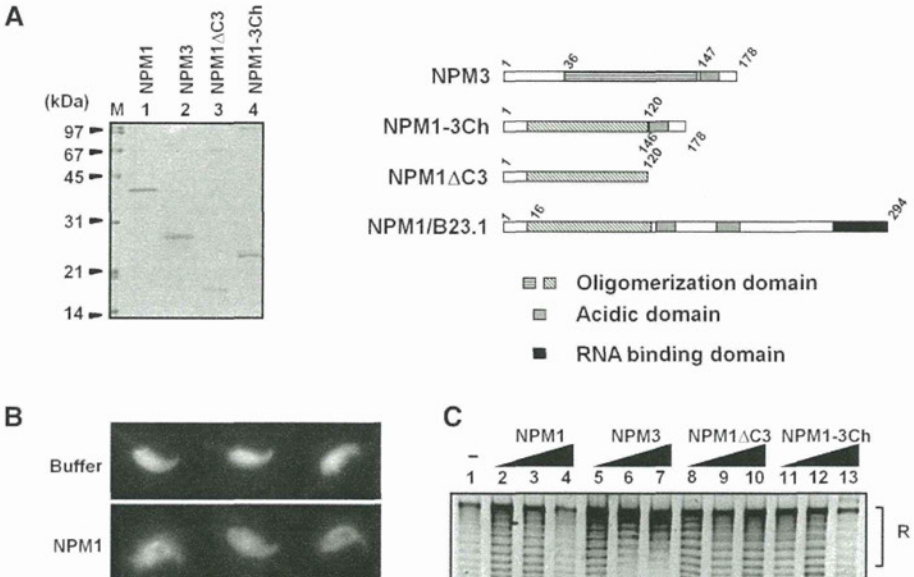

Figure 5. NPM3 functions as a histone chaperone when it forms an oligomer. (**A**) Purified recombinant proteins. His-tagged NPM1, NPM3, NPM1ΔC3 and NPM1–3Ch (lanes 1–4, respectively, 200 ng each) were separated by 12.5% SDS–PAGE and visualized with CBB staining. Because the oligomers of NPM1–3Ch and NPM1ΔC3 were not completely disrupted under SDS–PAGE condition, two bands, 18- and 70-kDa bands for NPM1ΔC3 and 25 and 100-kDa bands for NPM1–3Ch, were detected. The protein amounts of NPM1ΔC3 and NPM1–3Ch were estimated by the sum of two bands. The proteins used are schematically represented at the right side of the panel. The NPM1–3Ch protein is a fusion of NPM1(1–120) and NPM3(146–178). (**B**) Sperm chromatin decondensation activity. Mouse sperm nuclei were incubated in the absence or presence of NPM proteins (3 μg) at 37°C for 60 min, fixed, and stained with DAPI. Three typical sperm nuclei are shown. (**C**) Supercoiling assay. Core histones were incubated without or with increasing amounts of NPM1 (lanes 2–4), NPM3 (lanes 5–7), NPM1ΔC3 (lanes 8–10) and NPM1–3Ch (lanes 11–13) (100, 300 and 1000 ng for each protein). Then the topoisomerase I-treated plasmid DNA (100 ng) was added and incubated. DNA was purified and separated on 1% agarose gel electrophoresis in 1× TBE. Positions of supercoiled (S) and relaxed (R) plasmid DNA are shown at the right side of the panel.

molecules should be complexed with His-tagged NPM3. Purified proteins were further fractionated by Mono Q chromatography to remove excess His–NPM3 in the complex. The CBB-stained gel revealed that the ratio between NPM1:His–NPM3 in the complex was very similar to 4:1 (Figure 6C, lane 2). The complex was then subjected to gel filtration, and fractions were analyzed by western blotting (Figure 6D). As described previously, the masses of NPM1 and NPM2 were estimated to be 370 and 270 kDa, respectively. However, NPM1 was broadly distributed when complexed with His–NPM3 despite the masses of NPM1 peak fraction being similar to that of NPM1 alone. Taken together, we conclude that NPM1 and NPM3 preferentially form a 4:1 pentamer and two pentamers are assembled into decamers, and that NPM3 may have a role in destabilizing the NPM1 pentamer/decamer formation.

Next, we examined the function of the NPM1–NPM3 complex in sperm chromatin remodeling. As shown in Figure 7A, both NPM1 alone and the NPM1–NPM3 complex, but not NPM3, efficiently decondensed mouse sperm nuclei in incubation time-dependent manner. Similarly, the NPM1–NPM3 complex mediated nucleosome assembly, as did NPM1 (Figure 7B, lanes 2–4 and 8–10), while NPM3 did so less efficiently (lanes 5–7), indicating that NPM3 cooperates with NPM1 in the first and second steps of sperm chromatin remodeling during fertilization.

NPM1 and NPM3 are ubiquitously expressed, and their expression level is higher in actively growing cells than in quiescent cells. We therefore investigated the biological significance of NPM1 and NPM3 complex formation in growing cells. We previously demonstrated that RNA binding of NPM1 is required for efficient histone chaperone activity in the nucleolus (22). Thus, we tested the RNA-binding activity of the NPM1–NPM3 complex using a filter-binding assay (Figure 8B). The NPM1–NPM3 complex was prepared using GST–NPM1 and His–NPM3 (Figure 8A). GST–NPM1 alone or GST–NPM1 mixed with a 3-fold molar excess of His–NPM3 was denatured, and the proteins were refolded by extensive dialysis. Refolded proteins were further purified with glutathione sepharose to remove free His–NPM3 (lane 3). GST–NPM1 bound to radiolabeled RNA was retained on

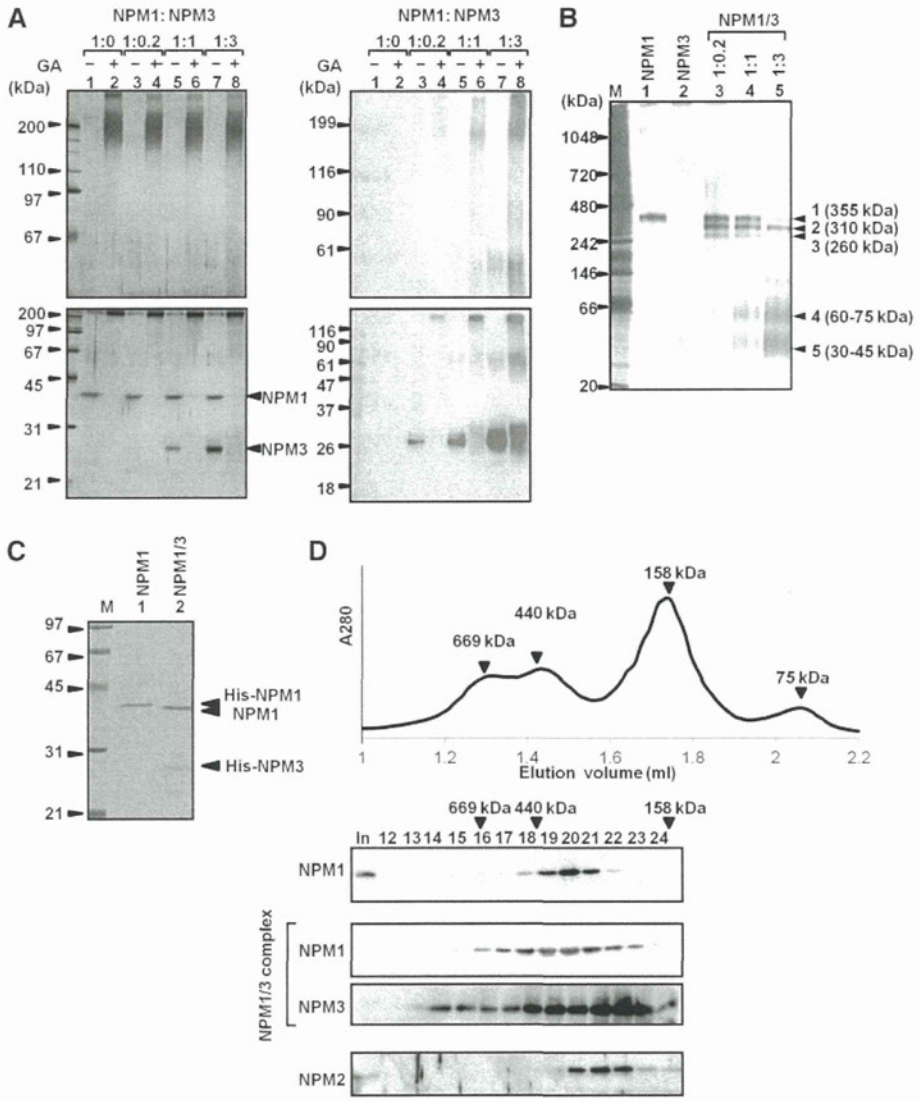

Figure 6. Oligomer formation between NPM1 and NPM3. (**A**) Crosslinking experiments. Recombinant His–NPM1 was mixed with increasing amounts of His–NPM3 (1:0 for lanes 1 and 2, 1:0.2 for lanes 3 and 4, 1:1 for lanes 5 and 6, and 1:3 for lanes 7 and 8), denatured in the buffer containing guanidine hydrochloride, and renatured by extensive dialysis. The mixtures were subjected to chemical crosslinking experiment with 0.05% GA. The mixtures treated without (lanes 1, 3, 5 and 7) or with (lanes 2, 4, 6 and 8) GA were separated on 7.5% and 12.5% SDS–PAGE (top and bottom panels, respectively) and visualized with silver staining (left panel) or western blotting with an anti-NPM3 antibody (right panel). Positions of molecular weight markers are indicated at the left, and those of free NPM1 and NPM3 are indicated at the right side of the panel. (**B**) BN–PAGE analysis of the NPM1–NPM3 complex. NPM1, NPM3 and NPM1–NPM3 complexes as in A were separated on 4–16% BN–PAGE and visualized with silver staining. Lane M is molecular weight markers. Masses of bands shown at the right side of the panel were estimated as in Figure 2B. (**C**) NPM1/His–NPM3 preparation. His-tagged NPM3 and NPM1 were coexpressed in *E. coli* and purified as described in 'Materials and Methods' section. His–NPM1 and NPM1–His–NPM3 complex were separated on 12.5% SDS–PAGE and visualized with CBB staining. Positions of His–NPM1, non-tagged NPM1 and His–NPM3 are indicated at the right side of the panel. (**D**) Gel filtration analysis of NPM proteins. His–NPM1 (5 μg), NPM1/His–NPM3 (5 μg NPM1) and His–NPM2 (5 μg) in 20 μl were loaded on Superose 6 PC 3.2/30 column and fractionated. Fractions 12–24 were analyzed by SDS–PAGE and western blotting. Molecular masses were estimated from the elution profile of marker proteins as shown at the top of the panel.

the membrane in a GST–NPM1 dose-dependent manner (lanes 2–5). The activity of the GST–NPM1/His–NPM3 complex was lower than that of GST–NPM1 alone (lanes 6–9). These results indicated that NPM3 incorporation into the NPM1 pentamer greatly impacted the RNA-binding activity of NPM1, although this incorporation did not completely abolish the RNA-binding activity of NPM1.

Given that the RNA-binding activity of NPM1 was important for its nucleolar localization and cellular mobility (32) and that NPM3 incorporation into the NPM1 pentamer decreased RNA-binding activity (Figure 8B), we hypothesized that NPM3 increases NPM1 mobility in the cell. To examine this, fluorescence recovery after photobleaching analysis was performed using HeLa cells that stably expressed EF–NPM1 or EF–NPM3.

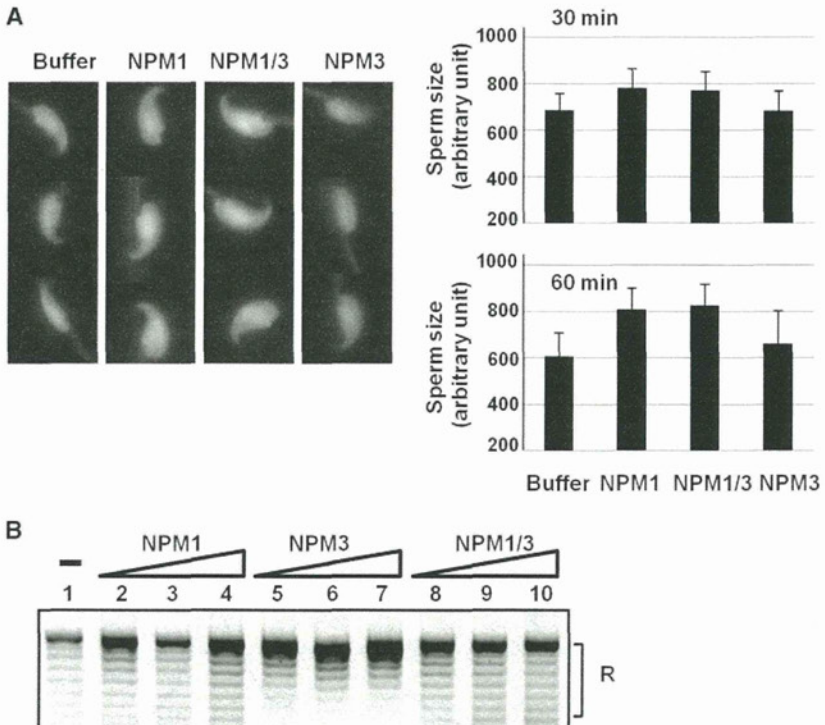

Figure 7. Sperm chromatin remodeling activity of the NPM1–NPM3 complex. (**A**) Sperm chromatin decondensation activity of the NPM1–NPM3 complex. Sperm nuclei in the absence or presence of His–NPM1, NPM1–His–NPM3 complex (NPM1/3), His–NPM3 prepared as in Figure 6C were incubated for 30 or 60 min. Sperm DNA was fixed and stained with DAPI, and observed by fluorescent microscopy. Three typical sperms (from 60 min incubation samples) are shown for each sample. Sperm nuclear size ($n > 30$) was estimated by Image J and averaged. Results are means ± SD. (**B**) Nucleosome assembly activity of the NPM1–NPM3 complex. Increasing amounts of His–NPM1, NPM3, and the NPM1–His–NPM3 complex (NPM1/3) (200, 600 and 2000 ng, for lanes 2–4, 5–7 and 8–10) were mixed with core histones (100 ng). Topo I-treated plasmid DNA (100 ng) was added and further incubated. DNA was purified, separated on 1% agarose gel and visualized with GelRed staining. Positions of relaxed (R) and supercoilied (S) DNA are indicated at the right side of the panel.

We confirmed that EF–NPM3 was efficiently depleted along with NPM1 from the nuclear extracts derived from HeLa cells that stably expressed EF–NPM3 (compare lanes 1–3 and 4–6 in Figure 8C). This result allowed us to test the mobility of a NPM1 oligomer containing NPM3 because NPM1 and NPM3 formed an oligomer (Figure 6) and most EF–NPM3 was complexed with NPM1 in cell extracts (Figure 8C). Thus, the observed mobility of EF–NPM3 localized in the nucleoli could represent the NPM1 complex containing EF–NPM3 molecule in the pentamer. For this experiment, the EGFP signal within a small nucleolus was targeted for bleaching with a 488-nm laser line. The intensity of the EGFP signal was measured every 0.5 s (Figure 8D). The recovery rate of NPM1 was rapid and the half time for fluorescence recovery ($t_{1/2}$) was calculated to be 7.10 ± 1.81 s. Under the same experimental condition, the $t_{1/2}$ of NPM3 was calculated to be 4.29 ± 1.21 s. These results strongly suggested that NPM3 incorporation into the pentamer increased the mobility of the NPM1 pentamer in the cell by restricting the RNA-binding activity of NPM1.

DISCUSSION

In this study, we characterized the sperm chromatin remodeling activity of three human NPM proteins. Sperm chromatin remodeling is divided into at least two reactions; the first step is chromatin decondensation by protamine removal, and the second step is assembly of nucleosomes with core histones. We systematically analyzed the function of human NPM proteins during both steps of sperm chromatin remodeling. We first demonstrated that NPM1 and NPM2 formed homo-pentamers in solution, whereas NPM3 mainly formed dimers (Figure 2). NPM3 showed significantly lower sperm chromatin decondensation and nucleosome assembly activities *in vitro* because of its inability to form a proper oligomer. Importantly, NPM3 efficiently mediated sperm chromatin remodeling when included in a pentamer containing NPM1 (Figure 7). The sperm chromatin remodeling activity of recombinant NPM2 was significantly lower than that of NPM1 (Figure 3). However, NPM2 activity was enhanced by phosphorylation at N-terminal region (Figure 4). These results suggest that all three NPM